Sophocleous Reece A (Orcid ID: 0000-0002-8339-9090)

Finol-Urdaneta Rocio K. (Orcid ID: 0000-0003-2157-4532)

Pharmacological and genetic characterisation of the canine P2X4 receptor

Running title: The canine P2X4 receptor

Reece A. Sophocleous[1,2], Tracey Berg[1,2], Rocio K. Finol-Urdaneta[1,3], Vanessa Sluyter[1,2], Shikara Keshiya[1,2], Lachlan Bell[1,2], Stephen J. Curtis[4], Belinda L. Curtis[4], Aine Seavers[5], Rachael Bartlett[1,2], Mark Dowton[1,2], Leanne Stokes[6], Lezanne Ooi[1,2] and Ronald Sluyter[1,2]

[1]Illawarra Health and Medical Research Institute, Wollongong, NSW 2522, Australia; [2]Molecular Horizons and School of Chemistry and Molecular Bioscience, University of Wollongong, Wollongong, NSW 2522, Australia; [3]Electrophysiology Facility for Cell Phenotyping and Drug Discovery, Wollongong, NSW 2522, Australia; [4]Albion Park Veterinary Hospital, Albion Park, NSW 2527, Australia; [5]Oak Flats Veterinary Clinic, Oak Flats, NSW 2529, Australia; [6]School of Pharmacy, University of East Anglia, Norwich NR4 7TJ, United Kingdom.

Word Count (excluding abstract, methods, references and figure legends)

Intro 460, Results 1820, Discussion, 1916

This article has been accepted for publication and undergone full peer review but has not been through the copyediting, typesetting, pagination and proofreading process which may lead to differences between this version and the Version of Record. Please cite this article as doi: 10.1111/bph.15009

Acknowledgments

This work was supported by the American Kennel Club Canine Health Foundation (Grant 01985). R.A.S. was supported through an Australian Government Research Training Program Scholarship. L.O. is supported by a National Health and Medical Research Council (NHMRC) of Australia Boosting Dementia Research Leadership Fellowship (APP1135720). We thank Margaret Phillips (University of Wollongong) and staff of the Illawarra Health and Medical Research Institute for technical assistance. We thank Professor Heath Ecroyd (University of Wollongong) for advice.

Ethics Statement

Informed consent was obtained from all pet owners. This work was approved by the Animal (protocols AE10/01 and AE14/09) and Human (protocol HE10/063) Ethics Committees of the University of Wollongong.

Conflict of Interest

The authors declare no conflict of interest.

Address for Correspondence

Professor Ronald Sluyter, School of Chemistry and Molecular Bioscience, University of Wollongong, Wollongong, NSW 2522, Australia.

E-mail: rsluyter@uow.edu.au

Abstract

Background and Purpose

The P2X4 receptor is an emerging therapeutic target for the treatment of chronic pain and cardiovascular disease. Dogs are well-recognised natural models of human disease but information regarding P2X4 in dogs is absent. To aid the development and validation of P2X4-targeting therapeutics, this study aimed to characterise and compare canine and human P2X4.

Experimental Approach

Genomic DNA was extracted from whole blood samples from 101 randomly selected dogs and sequenced across the *P2RX4* gene to identify potential missense variants. Recombinant canine and human P2X4 tagged with Emerald GFP were expressed in 1321N1 and HEK293 cells and analysed by immunoblotting and confocal microscopy. P2X4 pharmacology was characterised using nucleotide-induced Fura-2 AM measurements of intracellular Ca^{2+} responses and known P2X4 antagonists in 1321N1 and HEK293 cells. P2X4-mediated inward currents in HEK293 cells were assessed by automated patch clamp.

Key Results

No *P2RX4* missense variants were identified in any canine samples. Canine and human P2X4 were localised primarily to lysosomal compartments. ATP was identified as the primary agonist of canine P2X4 with near identical efficacy and potency at human P2X4. 2'(3')-O-(4-benzoyl)benzoyl ATP (BzATP), but not ADP, was identified as a partial agonist with reduced potency for dog P2X4 compared to the human orthologue. Five antagonists inhibited canine P2X4, with BX430 displaying reduced sensitivity and potency against canine P2X4.

Conclusion and Implications

P2X4 is highly conserved across dog pedigrees and displays a similar expression pattern and pharmacological profile to human P2X4, providing support for validation and use of therapeutics designed for P2X4-related disease onset and management in dogs and humans.

Key Words: P2X4, purinergic receptor, 5-BDBD, ivermectin, dog, calcium channel, single nucleotide polymorphism

Abbreviations: 5-BDBD, 5-(3-bromophenyl)-1,3-dihydro-2H-benzofuro[3,2-e]-1,4-diazepin-2-one; BX430, (1-(2,6-dibromo-4-isopropyl-phenyl)-3-(3-pyriudyl)urea; BzATP, 2′- & 3′-O-(4benzoylbenzoyl) ATP; ECS, extracellular Ca^{2+} solution; EmGFP, Emerald green fluorescent protein HRP, horseradish peroxidase; IVM, ivermectin; TNP-ATP, 2',3'-O-(2,4,6-trinitrophenyl) ATP.

Author contributions: R.A.S. designed and performed the majority of experiments, analysed all the data and wrote the manuscript. R.K.F-U. designed, conducted and analysed automated patch clamp experiments. R.S. conceived the study. R.S. and L.S. obtained funding for the study. T.B. generated the expression constructs. V.S., S.K., and L.B. performed additional gene sequencing. S.J.C., B.L.C. and A.S. provided canine blood samples and technical advice. S.K., L.B. and R.B. performed additional cell experiments. M.D. and L.S. provided technical advice. R.S. and L.O. supervised the project, designed experiments, reviewed the data and co-wrote the manuscript. All authors edited the manuscript.

Bullet point summary

What is already known

- P2X4 is expressed in humans and rodents with known roles in nociception and cardiovascular regulation.
- No data regarding functional canine P2X4 has been reported.

What this study adds

- Canine *P2RX4* encodes a functional ATP-gated Ca^{2+} channel with pharmacological similarities to human P2X4.
- The P2X4-selective inhibitor BX430 is less potent and sensitive against canine compared to human P2X4.

Clinical significance

- Compounds targeting human P2X4 also target canine P2X4 with similar effectiveness.
- Aids the validation of potential P2X4-targetting therapeutics for pre-clinical trials.

Introduction

P2X4 is a member of the ionotropic P2X receptors and forms homo-trimeric, ATP-gated Ca^{2+} channels in macrophages and glial cells (Trang & Salter, 2012; Tsuda, Tozaki-Saitoh *et al.*, 2010). Here it has important roles in signalling the release of prostaglandin E2 (Ulmann, Hirbec *et al.*, 2010) and brain-derived neurotrophic factor (Trang, Beggs *et al.*, 2009; Ulmann, Hatcher *et al.*, 2008), respectively. Elucidation of the role of P2X4 in these well-known nociceptive signalling pathways has led to suggestions that P2X4 is an attractive therapeutic target for the treatment of a number of major health issues such as inflammation and chronic pain (Bernier, Ase *et al.*, 2018), nerve injuries (Su, Wu *et al.*, 2019) and alcohol use disorder (Huynh, Arabian *et al.*, 2016). Functional P2X4 is also present on endothelial cells in humans and mice where it is associated with blood flow-dependent calcium signalling (Yamamoto, Korenaga *et al.*, 2000; Yamamoto, Sokabe *et al.*, 2006).

To date, two different missense variants in the gene coding P2X4 (*P2RX4*) have been associated with human disease. The missense Y315C variant (rs28360472) is significantly associated with increased pulse pressure (Stokes, Scurrah *et al.*, 2011). The same variant is associated with increased susceptibility to age-related macular degeneration when in linkage disequilibrium with a *P2RX7* missense G150R variant (rs28360447), which results in a reduction of P2X7-mediated phagocytosis by macrophages and microglia (Gu, Baird *et al.*, 2013). A second *P2RX4* variant (G135S; rs765866317) in a three-variant haplotype (together with the *P2RX7* variants T205M; rs140915863 and N361S; rs201921967) is associated with multiple sclerosis in a multi-incident family (Sadovnick, Gu *et al.*, 2017). As such, P2X4 has been proposed as a possible therapeutic target for the treatment of multiple sclerosis (Zabala, Vazquez-Villoldo *et al.*, 2018).

Despite the publication of high resolution crystal structures of zebrafish P2X4 (Hattori & Gouaux, 2012; Kawate, Michel *et al.*, 2009), researchers have struggled to identify potent and selective P2X4 antagonists (Tian, Abdelrahman *et al.*, 2014). However, in recent years, several commercially available antagonists with greater selectivity for P2X4 have appeared, although with disputed effectiveness. Data regarding P2X sub-type specificity and species-selectivity is incomplete (See Stokes, Layhadi *et al.*, 2017 for a review of current P2X4 antagonists). Overcoming species-specific pharmacological differences is a huge challenge faced by researchers developing drugs that target ion channels such as P2X4. Such

differences often hinder the translation of observations from pre-clinical animal models to humans. However, to date, the characterisation of canine P2X4 has not been reported.

To assist with pre-clinical validation of therapeutics for P2X4-related disease, canine P2X4 was synthesised and sub-cloned into a mammalian expression vector for functional characterisation, revealing a striking pharmacological similarity to human P2X4. Recently described human P2X4 antagonists were further characterised and their ability to inhibit Ca^{2+} flux through canine and human P2X4 was directly compared.

Methods

Genomic DNA isolation and sequencing

Canine peripheral blood was collected into VACUETTE lithium heparin tubes (Greiner Bio-One, Frickenheisen, Germany) from pedigree and non-pedigree dogs and studied in compliance with institutional (University of Wollongong) and ARRIVE guidelines. Genomic DNA was extracted from canine peripheral blood using the Wizard Genomic DNA Purification Kit (Promega, Madison, USA) according to manufacturer's instructions and stored at -80°C. Canine genomic DNA was amplified using forward and reverse primer pairs designed to intronic regions flanking between one and three exons of canine *P2RX4* as indicated (Supporting Table 1). PCR amplification was carried out using MangoTaq DNA polymerase with an initial denaturation at 95°C for 2 min, followed by 35-40 cycles of denaturation at 95°C for 30 s, annealing at 58.8-67°C for 30-60 s, and extension at 72°C for 1 min. After cycling was complete, a final extension was carried out at 72°C for 5 minutes then amplicons were incubated with ExoSAP-IT at 37°C for 15 minutes, followed by heat inactivation at 80°C for 15 minutes. *P2RX4* sequences from amplicons were determined using the respective primers listed in Supporting Table 1, the Applied Biosystems (Foster City, USA) ABI PRISM BigDye Terminator v3.1 Cycle Sequencing Kit and a 3130xl Genetic Analyser. Resulting sequence chromatograms were compared to the ENSEMBL reference gene transcripts for canine *P2RX4* described below.

Expression constructs

Synthetic canine and human *P2RX4* cloned into pUC57 plasmids were purchased from Sigma-Aldrich (St Louis, USA) and sub-cloned into a mammalian pEGFP-N3 vector with a C-terminal Emerald green fluorescent (EmGFP) tag connected by a 3x (-GGGGS-) flexible linker. Plasmid DNA was amplified by transformation into chemically competent DH5α (Thermo Fisher Scientific, Melbourne, Australia) bacterial cells and isolated using the Wizard Plus SV Minipreps DNA Purification kit (Promega, Madison, USA) according to manufacturer's instructions. Plasmid DNA was sequenced as above using primer pairs listed in Supporting Table 1. The canine and human *P2RX4* sequences obtained from these vectors were identical to their respective full length reference transcripts obtained from ENSEMBL (http://www.ensembl.org) (canine P2RX4-201 ENSCAFT00000013312.3; human P2RX4-202 ENST00000337233.8).

Cell lines

1321N1 human astrocytoma (ECACC Cat# 86030402, RRID:CVCL_0110) and HEK293 cells (ECACC Cat# 85120602, RRID:CVCL_0045) were maintained in DMEM/F12 medium containing 15% or 10% FBS, respectively, 2 mM GlutaMAX, 100 U mL^{-1} penicillin, 10 $\mu g.mL^{-1}$ streptomycin and 1% non-essential amino acids at 37°C/5% CO_2. Human cell line identities were confirmed through STR profiling (Garvan Molecular Genetics, Darlinghurst, Australia), and were routinely assessed for mycoplasma contamination using the MycoAlert Mycoplasma Detection Kit (Lonza, Waverley, Australia). Cells were plated at 3.5 x 10^5 cells per well in poly-D-lysine-coated 6-well plates (Greiner Bio-One, Frickenheisen, Germany) and transiently transfected the following day with canine or human P2X4-EmGFP, or the EmGFP empty vector (Sigma-Aldrich, St Louis, USA) using Lipofectamine3000 as per the manufacturer's instructions. Briefly, 0.4 µg of plasmid DNA, 5 µL of Lipofectamine reagent, 4 µL P3000 reagent and 250 µL Opti-MEM (per well of a 6-well plate transfection) were incubated at room temperature for 15 minutes prior to adding to cells. Post-transfection (24-48 h), cells were plated at 5 x 10^4 cells per well in black-walled µClear bottom, poly-D-lysine-coated 96-well plates (Greiner Bio-One) for Ca^{2+} flux assays, or at 1 x 10^5 cells per 18 mm poly-D-lysine-coated glass coverslip for confocal microscopy, and incubated at 37°C/5% CO_2 overnight .

Fura-2 calcium response assay

P2X4 activity was assessed using Fura-2 measurements of nucleotide-induced Ca^{2+} influx as described (Ma, Hui *et al.*, 2009). Unless stated otherwise, all assays and compound dilutions were carried out using a standard extracellular Ca^{2+} solution (ECS; 145 mM NaCl, 2 mM $CaCl_2$, 1 mM $MgCl_2$, 5 mM KCl, 13 mM glucose and 10 mM HEPES, pH 7.4). Cells were washed twice with ECS then pre-incubated with Fura-2 AM loading buffer (2.5 µM Fura-2 AM/0.2% pluronic acid in ECS) in the dark for 30 minutes at 37°C. Before recording fluorescence, excess Fura-2 loading buffer was removed and cells were washed with ECS then incubated for a further 20 minutes to allow for complete de-esterification. Fura-2 fluorescence emission at 510 nm was recorded every five seconds using a Flexstation3 (Molecular Devices, Sunnyvale, USA) following excitation at 340 and 380 nm (six reads per well, photomultiplier tube setting medium). Baseline recordings were taken for 15 seconds then following the addition of nucleotide or vehicle (up to a final volume of 100 µL per well), recordings were taken for up to three minutes. Where indicated, antagonists, ivermectin (IVM) or respective vehicle controls were added to each column of the 96-well assay plate at regularly-spaced two-minute intervals at 37°C. After 20 minutes of pre-incubation, Fura-2 fluorescence (as described above) was measured for 15 seconds then following the addition of ATP or vehicle (up to a final volume of 100 µL per well), recordings were taken for up to two minutes. Compound additions were carried out using the Flexstation3 built-in fluidics system. In some experiments, hexokinase (4.5 $U.mL^{-1}$) was incubated with 1.5 mM ADP (or ATP) in ECS for 60 minutes at 37°C prior to addition of nucleotides. Data were acquired using SoftMax Pro 7 software (Molecular Devices).

Automatic Planar Patch-Clamp Electrophysiology

HEK293 cells transfected with canine or human P2X4 were detached from 6-well plates using TrypLE and resuspended in cold external recording solution (140 mM NaCl, 5 mM Glucose, 4 mM KCl, 2 mM $CaCl_2$, 1 mM $MgCl_2$ and 10 mM HEPES, 298 ± 3 mOsm, pH 7.4 with NaOH) containing 1 U/mL apyrase. Cells were kept in suspension by automatic pipetting at 4°C. Patch-clamp measurements were performed on an NPC-16 Patchliner (Nanion Technologies, Munich, Germany) using multi-hole medium resistance NPC-16 chips with an average resistance of 1.1 MΩ. Recordings were made in the whole-cell configuration

with internal solution (60 mM CsF, 50 mM CsCl, 20 mM NaCl, 10 mM HEPES and 10 mM EGTA, 285 ± 3 mOsm, pH 7.2 with CsOH) and external recording solution in absence of apyrase. Seal formation was enhanced by brief treatment with SE seal enhancement solution (80 mM NaCl, 3 mM KCl, 10 mM $MgCl_2$, 35 mM $CaCl_2$ and 10 mM HEPES, 298 ± 3 mOsm, pH 7.3 with NaOH) until stable seals were obtained and replaced with standard external solution. Solutions were 0.2-μm membrane filtered. Recordings where seal resistance (SR) was >500MΩ and access resistance was <3xSR were considered acceptable. Chip and whole-cell capacitance were fully compensated, and series resistance compensation (70%) was applied via Auto Rs Comp function. Recordings were acquired with PatchMaster (HEKA Elektronik, Lambrecht/Pfalz, Germany) and stored on a computer running PatchControlHT software (Nanion Technologies GmbH, Munich, Germany). A test pulse in control bath solution application (0 ATP) was used to subtract leak currents. Offline analysis was performed using Igor Pro-6.37 (WaveMetrics Inc.). Solutions were puffed (~1 second) during a 5 second test pulse from a holding potential (Vh) of -70mV. The integer of area under the curve described by the inward currents in response to the ATP puff was used for quantification of agonist-induced responses, with concentration-response curves plotted as charge density (pC/pF) normalised to current at 1 mM ATP. All recordings were conducted at room temperature.

Confocal microscopy

Cells on glass coverslips were fixed with 3% paraformaldehyde at 4°C for 15 min then washed three times with PBS. Cells were permeabilised with 0.1% saponin in 2% BSA/PBS at room temperature for 15 min and then incubated with goat anti-P2X4 (1:250) (Sigma-Aldrich Cat# SAB2500734, RRID:AB_10604119, Lot# 8830P1) or mouse anti-LAMP1 (1:100) (DSHB Cat# H4A3, RRID:AB_2296838) antibodies in 2% BSA/PBS at room temperature for two hours. Cells were washed three times with PBS and then incubated with Alexa Fluor 594-conjugated donkey anti-goat (1:200) (Abcam Cat# ab150136, RRID:AB_2782994, Lot# GR308670-1) or PE-conjugated sheep anti-mouse (1:200) (Chemicon Cat# AQ326H, Lot# 985052005) antibodies in 2% BSA/PBS at room temperature for 60 minutes. Washed coverslips were mounted onto a glass slide using 50% glycerol in PBS and sealed with nail polish. Cells were visualised on a Leica (Mannheim, Germany) SP5 confocal microscope.

Western blotting

Cells (1 x 10^6) were washed three times with ice-cold PBS and harvested by mechanical scraping and centrifugation (300 x g for 5 min). Following incubation in complete lysis buffer (50 mM BisTris, 750 mM 6-aminohexanoic acid, 1 mM PMSF, 1% n-dodecyl β-D-maltoside and 1 cOmplete EDTA-free protease inhibitor cocktail tablet, pH 7.0) at 4°C with gentle agitation for 60 min, cells were sheared 10 times through an 18 gauge needle and centrifuged at 16,000 x g for 15 min at 4°C. Cell supernatants were separated by denaturing SDS-PAGE under reducing conditions (10 mM DTT) using Mini-Protean TGX Stain-Free gels (4-20%) then transferred onto a nitrocellulose membrane. The membrane was washed three times in Tris-buffered saline solution containing Tween-20 (TBST) (20 mM Tris, 500 mM NaCl, 0.1% Tween-20, pH 7.5) and blocked in blocking buffer (TBST containing 5% skim milk powder) for 60 min at room temperature. The membrane was then incubated overnight with goat anti-P2X4 (1:500) or rabbit anti-actin (1:2000) (Sigma-Aldrich Cat# A2066, RRID:AB_476693) antibodies in blocking buffer at 4°C. The membrane was washed three times for 5 min with TBST and incubated with horseradish peroxidase (HRP)-conjugated mouse anti-goat (Thermo Fisher Scientific Cat# 31400, RRID:AB_228370, Lot# KC1205131) or goat anti-rabbit IgG (Rockland Cat# 611-103-122, RRID:AB_218567, Lot# 21231) (both 1:5000) antibodies in blocking buffer at room temperature for 60 min. The membrane was washed as above and visualised using chemiluminescent substrate and an Amersham Imager 600RGB (GE Healthcare Lifesciences). The experimental detail for all western blots provided conforms with the *BJP* guidelines (Alexander, Roberts *et al.*, 2018).

Data and statistical analysis

The relative change in intracellular Ca^{2+} (ΔCa^{2+}) data was expressed as the ratio of Fura-2 fluorescence following excitation at 340 nm and 380 nm ($F_{340/380}$) then normalised to the mean basal fluorescence according to the formula $\Delta Ca^{2+} = \Delta F/F = (F - F_{rest})/F_{rest}$, where F is the $F_{340/380}$ at a given time and F_{rest} is the mean fluorescence of the given well prior to the addition of nucleotides (Paredes, Etzler *et al.*, 2008). Nucleotide-induced ΔCa^{2+} responses were then calculated by subtracting the ΔCa^{2+} response in absence of the respective nucleotide (measured simultaneously). To minimise potential caveats of high-throughput fluorescence-based assays such as large, erroneous ΔCa^{2+} measurements (Heusinkveld & Westerink, 2011), peak nucleotide-induced ΔCa^{2+} responses were defined by the median of

five readings surrounding the peak nucleotide-induced ΔCa^{2+} response. To control for plate-to-plate variation over time and slight variations in P2X4 expression, the peak nucleotide-induced ΔCa^{2+} response was normalised to the response to 10 μM ATP alone (percent of maximum), which was measured for both canine and human P2X4 for each independent experiment. Agonist concentration-response curves were plotted by a non-linear regression fit to the Hill equation using the least squares method, following a replicates test to confirm adequate fit of the curve. Half-maximal responses are expressed as their negative logarithm (pEC_{50}/pIC_{50}) ± SEM. Unpaired two-tailed Student's t-test or two-way ANOVA with Bonferroni *post hoc* test were used as indicated in the Figure and Table legends where group size was equal to at least five independent values (with two or more technical replicates per sample to ensure the reliability of single values), there was no significant variance in homogeneity (Bartlett's or F test for equal variance) and the data followed a Gaussian distribution (determined by a D'agostino-Pearson omnibus K2 test). Any data with less than five independent values were not subject to statistical comparisons. A non-parametric Mann-Whitney U test was carried out to compare differences when data were normalised to a 100% control with no variance. Curve fitting and statistical comparisons were made using GraphPad Prism 5 (GraphPad Software, San Diego, CA). Co-localisation analysis and calculation of Pearson's coefficient was performed using the JACoP (Just Another Co-localization Plugin) tool for ImageJ. Differences between *P2RX4* variant prevalence were compared using the Fisher's Exact test. For determining differences between groups, $P < 0.05$ was considered statistically significant throughout the entire manuscript and statistical analysis was carried out only on independent values, including any outliers. Assays and data analysis were performed unblinded and non-randomised, however where possible, plate structure was routinely altered to mitigate positioning bias within data sets. The data and statistical analysis comply with the recommendations on experimental design and analysis in pharmacology (Curtis, Alexander *et al.*, 2018).

Materials, compounds and solutions

DMEM/F12 medium, ExoSAP-IT, Fura-2 AM, GlutaMAX, HRP-conjugated anti-goat antibody, Lipofectamine3000, Opti-MEM I reduced serum medium, penicillin-streptomycin, ExoSAP-IT, Subcloning Efficiency™ DH5α™ Competent Cells, TrypLE Express and trypsin-EDTA were from Thermo Fisher Scientific (Melbourne, Australia). ABI PRISM

BigDye Terminator v3.1 Cycle Sequencing Kit was from Applied Biosystems (Carlsbad, USA). MangoTaq DNA polymerase was from Bioline (London, UK). HRP-conjugated anti-rabbit IgG antibody was from Rockland Immunochemicals (Pottstown, USA). Mini-Protean TGX Stain-Free™ gels, Precision Plus Protein™ Dual Colour standards and nitrocellulose membrane were from Bio-Rad (Hercules, USA). Alexa Fluor 594-conjugated donkey anti-goat IgG antibody was from Abcam (Melbourne, Australia). PE-conjugated sheep anti-mouse IgG antibody was from Chemicon (Boronia, Australia). Mouse anti-LAMP1 antibody (H4A3) was from the Developmental Studies Hybridoma Bank (Iowa City, USA). FBS (heat-inactivated) was from Bovogen Biologicals (East Keilor, Australia). Wizard Genomic DNA Purification and Wizard Plus SV Minipreps DNA Purification kits were from Promega (Madison, USA). 6-Aminohexanoic acid, ADP (sodium salt, cat. no. A2754), apyrase (cat. no. A6535), ATP (disodium salt, cat. no. A7699), 2'(3')-O-(4-benzoyl)benzoyl ATP (BzATP; triethylammonium salt, cat. no. B6396), cOmplete™ EDTA-free protease inhibitor cocktail, n-dodecyl β-D-maltoside, DMSO, (S)-duloxetine (HCl, cat. no. SML0474), EGTA, goat anti-P2X4 antibody (SAB2500734), hexokinase from *Saccharomyces cerevisae* (cat. no. H4502), IVM (cat. no. 18898), MEM non-essential amino acid solution, paroxetine (maleate salt, cat. no. P1372), PBS, pluronic F-127, PMSF, poly-D-lysine hydrobromide (5 $\mu g.mL^{-1}$ working stock), rabbit anti-actin antibody and saponin were from Sigma-Aldrich (St. Louis, USA). 5-(3-Bromophenyl)-1,3-dihydro-2H-benzofuro[3,2-e]-1,4-diazepin-2-one (5-BDBD; cat. no. 3579), 1-(2,6-dibromo-4-isopropyl-phenyl)-3-(3-pyriudyl)urea (BX430; cat. no. 5545), 2',3'-O-(2,4,6-Trinitrophenyl)-ATP (TNP-ATP; tetra(triethylammonium) salt, cat. no. 2464) and AR-C118925 (cat. no. 4890) were from Tocris Bioscience (Bristol, UK). BSA, EGTA and reagents for preparing buffers were from Sigma-Aldrich or Amresco (Solon, USA). Primers for sequencing were obtained from GeneWorks (Hindmarsh, Australia) or Integrated DNA Technologies (Coralville, USA).

Compounds were initially made up to stock concentrations in either Milli-Q H_2O (100 mM ATP (pH 7.4 with 5 M NaOH), 30 mM ADP, 40 mM BzATP, 10 mM duloxetine and 10 mM TNP-ATP) or DMSO (10 mM 5-BDBD, 30 mM BX430, 30 mM paroxetine, 3 mM IVM and 30 mM AR-C118925). Compounds were stored at -20°C, and then diluted in ECS for Ca^{2+} response assays or standard external solution for patch clamp recordings on the day of use, performed unblinded by the experimenter. DMSO controls for each compound (up to 1% in ECS) did not appear to have an effect on ATP-induced Ca^{2+} responses.

Nomenclature of targets and ligands

Key protein targets and ligands in this article are hyperlinked to corresponding entries in http://www.guidetopharmacology.org, the common portal for data from the IUPHAR/BPS Guide to PHARMACOLOGY (Armstrong, Faccenda *et al.*, 2020), and are permanently archived in the Concise Guide to PHARMACOLOGY 2019/2020 (Alexander, Mathie *et al.*, 2019).

Results

Genetic characterisation of canine P2X4

To determine the presence of exonic variants in canine *P2RX4*, genomic DNA samples from a randomly selected cohort of 101 dogs were isolated and sequenced using Sanger sequencing. The cohort consisted of 69 pedigree dogs (representing 32 different pedigrees) and 32 non-pedigree dogs (Supporting Table 2). Approximately 85% of the protein-coding region of *P2RX4* for this cohort was sequenced; some regions of various samples could not be amplified or sequenced despite three separate attempts. A query of the NCBI dbSNP, the EMBL-EBI European Variation Archive (EVA) and the iDOG databases (last accessed March 2019) revealed three reported missense variants; one in the first exon of *P2RX4* (no rsID, 26C>A, A9D; EVA database), one in exon seven (no rsID, 691C>T, R231C; EVA database) and one in exon ten (rs852294963, 1033C>G, L345V; NCBI dbSNP database). However, these three reported variants were not observed in our cohort, nor were any novel missense variants identified (Table 1). Several synonymous variants are also reported in the iDOG database (Supporting Table 3), however only rs852444127 (798C>T, T266T) was identified in our cohort and then only in heterozygous dosage in two Labrador retrievers and one beagle (Table 1). A previously unreported synonymous variant (15C>T) resulting in an unchanged cysteine at position five (C5C) was found in our cohort in heterozygous dosage only in both pedigree dogs (n = 5) and non-pedigree dogs (n = 3) (Table 1), four of which were of Maltese pedigree. This variant was absent in two other Maltese, whilst exon 1 could not be amplified in a further four Maltese. Both the allele frequency (0.33 and 0.04) and prevalence (66% and 7%) of this variant were significantly different between dogs of Maltese and non-Maltese pedigree, respectively. Combined this data indicates that the C5C variant may be associated with, but not limited to, dogs of Maltese pedigree.

Sequence identity of canine P2X4

The canine P2X4 amino acid sequence was compared to six cloned P2X4 orthologues (Table 2). Canine P2X4 had the highest sequence identity (90%) to human P2X4 (Table 2) with the highest regions of sequence identity occurring around and within the transmembrane domains (Figure 1A). A single M348V substitution exists within the second transmembrane domain of canine P2X4, the only difference between the transmembrane domains of canine and human P2X4 (Figure 1A). A stretch of 45 amino acids from P176 to A221, which contain a number of residues that form the ATP-binding sites of P2X4 (Chataigneau, Lemoine *et al.*, 2013) are also conserved between the mammalian species (Figure 1A). P2X4 sequences are relatively well conserved between canine and four other mammalian P2X4 orthologues (>85%), but this sequence identity drops below 70% (*Xenopus*) and 60% (zebrafish) when compared to taxa outside of the mammalian lineage (Table 2, Figure 1B).

Expression and localisation of cloned canine P2X4

Human and rodent P2X4 localises primarily to lysosomal compartments (Huang, Zou *et al.*, 2014; Stokes & Surprenant, 2009). To determine the sub-cellular localisation of canine P2X4, 1321N1 cells were transfected with canine or human P2X4-EmGFP constructs and analysed by confocal microscopy. 1321N1 cells transfected with canine or human P2X4-EmGFP revealed a distinct vesicular localisation and to a lesser extent cell-surface expression, both of which were similar for canine and human P2X4, visualised either by the EmGFP-tag (Figure 2A, Supporting Figure 1) or an anti-P2X4 antibody (Supporting Figure 1). In contrast, 1321N1 cells transfected with the EmGFP empty vector did not display a distinct vesicular localisation (cytoplasmic/nuclear distribution) nor were immunolabeled with the anti-P2X4 antibody at levels above the background fluorescence. Furthermore, both canine and human P2X4 appeared to co-localise with lysosomes (Pearson's coefficient = 0.735 and 0.610, respectively) revealed by anti-LAMP1 antibody labelling (Figure 2A). Western blot analysis of transfected 1321N1 cells confirmed the presence of a ~80 kDa band corresponding to the glycosylated P2X4 α-subunit (~55 kDa) plus EmGFP-tag (27 kDa) in transfected, but not wild type or EmGFP-transfected 1321N1 cells (Figure 2B), validating the use of this antibody for future studies of canine and human P2X4. Similar results were observed for HEK293 cells transfected with canine or human P2X4-EmGFP constructs (Supporting Figure 2A, B).

Pharmacological characterisation of canine P2X4 agonists

To pharmacologically characterise canine P2X4, the Ca^{2+} permeability properties of P2X4 channels were used to measure increases in intracellular Ca^{2+} bound to the ratiometric, fluorescent dye, Fura-2. Incubation with 10 □M ATP or 300 □M BzATP induced rapid Ca^{2+} responses which peaked within 10-30 seconds of application, followed by a slowly declining, sustained period, which was not observed upon addition of ECS vehicle alone (Figure 3A, B). Furthermore, these nucleotides evoked peak Ca^{2+} responses only in 1321N1 cells transfected with canine or human P2X4-EmGFP, but not with the EmGFP expression vector alone (Figure 3C).

ATP was the most potent agonist of canine P2X4 (Table 3), evoking a concentration-dependent Ca^{2+} response with maximal activity near 10 µM (Figure 3D). ATP produced a similar pharmacological profile in 1321N1 cells expressing human P2X4 (Figure 3E). BzATP also induced concentration-dependent Ca^{2+} responses in 1321N1 cells expressing canine and human P2X4, although with reduced potency towards canine P2X4 (Figure 3D, E). Peak Ca^{2+} responses achieved with 300 µM BzATP at canine and human P2X4 were 41 ± 7% and 92 ± 14% of 10 µM ATP, respectively. Unlike ATP, there was a significant difference in EC_{50} for BzATP between canine and human P2X4 (Table 3). Unexpectedly, ADP induced concentration-dependent Ca^{2+} responses in cells expressing canine and human P2X4 (Figure 3F, G), however, previous studies have reported that commercial stocks of ADP can contain small amounts of ATP (Mahaut-Smith, Ennion *et al.*, 2000). Therefore, ADP (and ATP as a positive control) was pre-incubated with hexokinase to remove contaminating ATP which resulted in significantly reduced ADP-induced Ca^{2+} responses in canine and human P2X4 transfected 1321N1 cells (Figure 3F, G). These experiments support previous reports of ATP contamination in ADP stocks and suggest that this contaminating ATP may account for the unexpected Ca^{2+} response to ADP.

To extend these findings, P2X4-mediated Ca^{2+} response agonist profiles were also characterised in HEK293 cells, a commonly used cell line for studying heterologously expressed P2X receptors (Jiang & Roger, 2020). Canine and human P2X4-transfected HEK293 cells displayed similar Ca^{2+} response agonist profiles (Figure 4A-D) to those observed for transfected 1321N1 cells (ATP pEC_{50} canine 6.09 ± 0.04, human 6.47 ± 0.03; BzATP pEC_{50} canine < 3, human 4.14 ± 0.06). Furthermore, electrophysiological characterisation of canine and human P2X4-mediated responses by automated patch clamp

recordings in HEK293 cells was consistent with our Ca^{2+} response data. Robust inward currents were activated with a charge density of 21 ± 7 and 34 ± 16 pC/pF at 100 µM ATP for canine and human P2X4, respectively (Figure 4E, F). This resulted in similar ATP response profiles in HEK293 cells transfected with canine (pEC_{50} of 5.02 ± 0.11) and human P2X4 (pEC_{50} 5.17 ± 0.10) (Figure 4E-G). No inward currents were elicited by 300 µM ATP in patch clamped mock EmGFP-transfected HEK293 cells (Supporting Figure 3A), yet ATP-induced Ca^{2+} responses were observed in EmGFP-transfected HEK293 cells (Supporting Figure 3B) consistent with the activity of endogenous metabotropic P2Y2 receptors reported previously in these cells (Schachter, Sromek *et al.*, 1997). Further investigation of HEK293 cells transfected with EmGFP vector alone in the absence or presence of 2 mM EGTA (to chelate extracellular Ca^{2+}) or 10 µM AR-C118925 (a P2Y2-selective inhibitor) showed that the observed ATP-induced Ca^{2+} response was partially reduced (53 ± 6.4%) in the presence of EGTA and almost completely reduced (90.6 ± 5.4%) upon AR-C118925 treatment (Supporting Figure 3C). Therefore, further characterisation of Ca^{2+} responses was limited to P2X4-expressing 1321N1 cells.

Ivermectin potentiates ATP-induced Ca^{2+} flux through canine P2X4

Ivermectin (IVM) is an allosteric modulator of human and rodent P2X4 (Khakh, Proctor *et al.*, 1999; Priel & Silberberg, 2004), but its effect on canine P2X4 is unknown. In order to determine if IVM is also a positive allosteric modulator of canine P2X4, cells expressing canine or human P2X4 were incubated in the presence or absence of 3 µM IVM (Priel & Silberberg, 2004) prior to activation with increasing concentrations of ATP. IVM significantly potentiated peak Ca^{2+} responses observed at 0.1 and 0.3 µM ATP in 1321N1 cells expressing canine (Figure 5A, B) or human (Figure 5C, D) P2X4, resulting in 2.9- and 1.7-fold decreases in the ATP EC_{50} for each orthologue, respectively (Table 3). Consistent with these results, ATP-induced inward currents recorded in HEK293 cells expressing canine P2X4 were potentiated by 1 µM IVM as demonstrated by a 2.0- to 2.5-fold increase in charge density following increased peak inward currents and marked decreases in desensitisation kinetics (Supporting Figure 4A, B). The current enhancement observed during our automated patch clamp characterisation of canine P2X4-mediated currents supports previous whole-cell patch clamp recordings of human P2X4 obtained in the presence of IVM (Priel & Silberberg, 2004).

Characterisation of canine P2X4 antagonists

A number of human and rodent P2X4 antagonists have been identified, but no data has been published to date regarding their effect on canine P2X4. To address this, Ca^{2+} responses in 1321N1 cells transfected with canine P2X4 were assessed using two P2X4-selective antagonists (BX430 and 5-BDBD), as well as three non-selective antagonists of human or rodent P2X4 (duloxetine, paroxetine and TNP-ATP) (Stokes, Layhadi *et al.*, 2017). At 0.75 µM ATP (corresponding to the approximate EC_{80}), all five antagonists demonstrated concentration-dependent inhibition of both peak and sustained ATP-induced Ca^{2+} responses of canine and human P2X4 (Figure 6A-J). Moreover, with the exception of BX430 and paroxetine, each compound displayed similar efficacy against canine and human P2X4 (Figure 6K-O, Table 3). The P2X4-selective antagonist BX430 was less active against canine P2X4 at concentrations greater than 3 µM resulting in a significant reduction in potency compared to human P2X4 (Figure 6K, Table 3). In contrast, the non-selective inhibitor paroxetine displayed significantly greater potency against canine P2X4 when compared to human P2X4 (Figure 6N, Table 3). However, unlike BX430, higher concentrations of paroxetine appear to have comparable inhibitory effects at canine and human P2X4.

Given the similarity in efficacy of the P2X4-selective antagonist 5-BDBD between canine and human P2X4 (Figure 6L), and its increasing use in studies of P2X4 activity, the mechanism of inhibition of 5-BDBD was further assessed against maximal concentrations of P2X4 agonists. 1321N1 cells transfected with canine or human P2X4 were pre-incubated in the presence or absence of 30 µM 5-BDBD and then activated with 10 µM ATP or 300 µM BzATP. However, despite previously observing inhibition of ATP-induced Ca^{2+} responses with 0.75 µM ATP (~EC_{80}, Figure 6L), 5-BDBD failed to reduce canine or human P2X4 Ca^{2+} responses evoked by saturating concentrations of 10 µM ATP (Figure 7A). In contrast, 5-BDBD caused a significant reduction in Ca^{2+} responses evoked by 300 µM BzATP in cells expressing canine or human P2X4 (81 ± 8% and 48 ± 7% reduction, respectively) (Figure 7B). Taken together, the data presented in Figures 6K and 7A are consistent with 5-BDBD being a more potent inhibitor of P2X4 at sub-saturating concentrations of ATP, consistent with a competitive mode of inhibition. Accordingly, 300 µM BzATP-induced P2X4 responses were effectively blocked by 5-BDBD, suggesting that BzATP at this concentration does not saturate P2X4 from either species.

Discussion

The current study described for the first time, the pharmacology of canine P2X4 and indirectly supports the concept that dogs express functional P2X4. Canine P2X4 displayed similar *in vitro* pharmacology to that of human P2X4, with two notable differences: canine P2X4 was less sensitive to activation by BzATP and to inhibition by BX430. Our work revealed that canine P2X4, like human P2X4, largely resides within intracellular compartments that are immunoreactive to LAMP1 consistent with lysosomal localisation. Concurrently, we also show that the protein coding region of the *P2RX4* gene is highly conserved amongst dogs.

It was determined here that ATP and BzATP are agonists and partial agonists of canine P2X4, respectively. Under our experimental setting, the EC_{50} for ATP was similar for both canine and human P2X4, consistent with previously published EC_{50} values for human, mouse and rat P2X4 (Abdelrahman, Namasivayam *et al.*, 2017; Garcia-Guzman, Soto *et al.*, 1997; Jones, Chessell *et al.*, 2000; Layhadi, Turner *et al.*, 2018; Soto, Garcia-Guzman *et al.*, 1996). Given the high sequence identity between canine and human P2X4 (90%), it was not unexpected to identify similar pharmacological profiles towards ATP. This is supported by studies demonstrating conservation of crucial ATP-binding residues (underlined in Figure 1) across P2X sub-types (Chataigneau, Lemoine *et al.*, 2013; Jiang, Rassendren *et al.*, 2000; Roberts, Digby *et al.*, 2008) and amongst human and rodent P2X4 (Abdelrahman, Namasivayam *et al.*, 2017). The BzATP EC_{50} reported here for canine P2X4 is consistent with that reported for rat P2X4 (EC_{50} > 100 µM), but not human or mouse P2X4 (Abdelrahman, Namasivayam *et al.*, 2017). The data reported here also suggests that BzATP is a partial agonist of human P2X4, in agreement with previous studies (Abdelrahman, Namasivayam *et al.*, 2017; Bianchi, Lynch *et al.*, 1999; He, Gonzalez-Iglesias *et al.*, 2003). The reasons for observed differences in BzATP sensitivity between species are yet to be fully understood but may be attributed to variations in BzATP-sensitive residues between species leading to less-favourable binding conformations (Browne, Jiang *et al.*, 2010; Pasqualetto, Brancale *et al.*, 2018; Tvrdonova, Rokic *et al.*, 2014).

The current study demonstrated that ADP is not an agonist of canine P2X4 as reported for human P2X4 in which 100 µM ADP failed to elicit significant responses (Garcia-Guzman, Soto *et al.*, 1997). However, subsequent studies report ADP acting as a P2X4 partial agonist (Bianchi, Lynch *et al.*, 1999; Carpenter, Meadows *et al.*, 1999; He, Gonzalez-Iglesias *et al.*,

2003). Such discrepancies may be due to the presence of ATP contamination in commercially available ADP stocks (Mahaut-Smith, Ennion *et al.*, 2000). Thus, consistent with previous studies (Micklewright, Layhadi *et al.*, 2018), ADP was pre-incubated with hexokinase to remove any contaminating ATP, which revealed negligible ADP-induced Ca^{2+} responses in 1321N1 cells expressing recombinant canine or human P2X4. Thus, as reported by Garcia-Guzman and colleagues (1997) for human P2X4, ADP does not activate canine P2X4. Moreover, caution should be taken when attributing ADP effects on ATP-responsive P2 receptors when using commercially obtained stocks.

The current study reported IVM as a positive modulator of canine P2X4. This commonly used anti-parasitic drug resulted in significant increases in the efficacy of ATP at canine and human P2X4. This increase is consistent with previous reports that IVM positively modulates human P2X4 (Priel & Silberberg, 2004). Moreover, the positive modulation of canine P2X4 by IVM is supported by conservation of critical residues for IVM recognition and binding such as Trp46, Trp47, Val60 and Val357 (Jelinkova, Yan *et al.*, 2006; Popova, Trudell *et al.*, 2013). The evidence presented here regarding canine P2X4 sensitivity to IVM, coupled with the frequent use of IVM as a preventative treatment for heartworm in dogs, provides a strong platform for dogs as natural models of human disease. Recently, IVM has been proposed as a potential P2X4-active drug for the treatment of demyelinating diseases like multiple sclerosis (Zabala, Vazquez-Villoldo *et al.*, 2018), however such diseases are seldom reported in domestic dogs (Vandevelde & Zurbriggen, 2005). Observations of canine health following life-long treatment with IVM could provide valuable insight as to the effect of targeting P2X4 for treatment or prevention of associated diseases such as multiple sclerosis in humans.

The current study has shown that three non-selective compounds, duloxetine, paroxetine and TNP-ATP, can inhibit canine P2X4. The selective serotonin reuptake inhibitor, paroxetine, and the serotonin-norepinephrine reuptake inhibitor, duloxetine, are reported to non-selectively inhibit human and rodent P2X4 (Nagata, Imai *et al.*, 2009; Yamashita, Yamamoto *et al.*, 2016), as well as to alleviate allodynia in models of chronic pain (Iyengar, Webster *et al.*, 2004; Zarei, Sabetkasaei *et al.*, 2014). Consistent with these previous studies, both compounds demonstrated effective inhibition of canine and human P2X4, albeit at relatively high concentrations (>100 μM). Moreover, the broad-spectrum P2X receptor antagonist TNP-ATP blocked canine and human P2X4 with similar potency, which agrees with previous work describing TNP-ATP as an antagonist of human and rodent P2X4 (Abdelrahman,

Namasivayam *et al.*, 2017; Nagata, Imai *et al.*, 2009). These compounds lack selectivity for P2X4 and as such, their use for studying canine P2X4 may be limited. However, given that duloxetine and paroxetine are approved human drugs, they may provide potential therapeutic benefits in dogs, in which P2X4 may be implicated.

This study also demonstrated that two selective inhibitors of P2X4, BX430 and 5-BDBD, can inhibit canine P2X4. The data presented here identified the phenylurea BX430 as a moderately potent antagonist of canine P2X4, although with a four-fold higher IC_{50} than for human P2X4. This is consistent with species differences reported with BX430 where this compound has displayed potent inhibition of human and bovine P2X4, moderate inhibition of zebrafish and *Xenopus* P2X4, and no inhibition of rodent P2X4 (Ase, Honson *et al.*, 2015; Ase, Therrien *et al.*, 2019). Ase and colleagues (2019) have attributed this difference to a single P2X4 residue (Ile312 human numbering, highlighted green in Figure 1A) which forms a docking site with Asp88 and Tyr300 and plays a crucial role in determining sensitivity to BX430. The conservation of this docking site between P2X4 orthologues such as canine, human and zebrafish and the apparent differences in sensitivity to BX430 may indicate a role for additional residues in mediating the inhibitory effects of BX430.

In contrast, the benzodiazepine derivative 5-BDBD inhibited canine and human P2X4 with similar potency but with limited effectiveness compared to other inhibitors. Consistent with this data, 5-BDBD has been reported as a moderately potent inhibitor of human and rodent recombinant P2X4, with limited effectiveness at sub-micromolar concentrations (Abdelrahman, Namasivayam *et al.*, 2017; Ase, Honson *et al.*, 2015; Balazs, Danko *et al.*, 2013; Coddou, Sandoval *et al.*, 2019). The data presented here is also in agreement with recent studies demonstrating inhibition of endogenous P2X4 activity in human monocyte-derived macrophages (Layhadi & Fountain, 2017) and human $CD4^+$ T cells (Ledderose, Liu *et al.*, 2018). Furthermore, the current study reported 5-BDBD to be ineffective at inhibiting Ca^{2+} responses induced by saturating concentrations of ATP. This is consistent with reports describing 5-BDBD as a competitive inhibitor of P2X4 assessed by radioligand binding assays (Balazs, Danko *et al.*, 2013) suggesting that this compound may have an allosteric inhibitory mechanism (Abdelrahman, Namasivayam *et al.*, 2017). Nonetheless, the limited potency and efficacy of BX430 and 5-BDBD highlights the need to identify more potent, selective P2X4 antagonists for treating disease in humans and dogs.

The current study also demonstrated that canine P2X4, like human and rodent P2X4, is predominantly localised to intracellular compartments of cells, with limited expression at the plasma membrane. Consistent with what has previously been shown for human and rodent P2X4 (Huang, Zou *et al.*, 2014; Stokes & Surprenant, 2009), canine P2X4 co-localised with LAMP1-labelled lysosomes. This data is further supported by observations that di-leucine ($L_{22}I_{23}$) and tyrosine-based (Y_{372}xxV and Y_{378}xxGL) endo-lysosomal targeting motifs (Qureshi, Paramasivam *et al.*, 2007) are conserved in canine P2X4. Moreover, expression of functional canine P2X4 on lysosomal compartments supports growing evidence for a physiological role of P2X4 in lysosomal membrane trafficking and fusion (Murrell-Lagnado & Frick, 2019). In addition, despite transfection with equal amounts of plasmid DNA, the Ca^{2+} response and current magnitude for human P2X4 were repeatedly higher than those for canine P2X4. This difference likely reflects differences in transcription and translation rates of canine and human P2X4, or the expression of a canine protein in a human cell line. Notably, uncharacterised effects on ion channel physiology and/or pharmacology arising from attachment of EmGFP to the C-terminal of P2X4 cannot be discarded despite representing a common approach utilised in functional characterisation (Sadovnick, Gu *et al.*, 2017).

The current study determined that the coding sequence of *P2RX4* is highly conserved amongst 101 dogs. The lack of genetic variation in canine *P2RX4* contrasts that of canine *P2RX7* (Sophocleous, Sluyter *et al.*, 2019; Spildrejorde, Bartlett *et al.*, 2014) which encodes four characterised missense variants. The difference between canine *P2RX4* and *P2RX7* parallels the frequencies of missense variants between human *P2RX4* (Stokes, Scurrah *et al.*, 2011) and *P2RX7* (Stokes, Fuller *et al.*, 2010). Since the publication of the canine genome (Lindblad-Toh, Wade *et al.*, 2005), few missense *P2RX4* variants have been reported in canine genome databases (dbSNP, EVA, iDOG,), however none so far have been validated by publication or characterised in functional studies. Nonetheless, the reduced polymorphic variation in canine *P2RX4* compared to human *P2RX4* is consistent with current observations of genome-wide loss in genetic variation due to domestication and selective breeding (Ostrander, Wayne *et al.*, 2017). Currently, there are around 400 recognised domestic pedigrees worldwide (Ostrander, Wayne *et al.*, 2017). With such a diverse range of pedigrees worldwide, there is potential for regional or pedigree bias within the present study, with Labrador, Staffordshire and Maltese associated pedigrees collectively forming over one third of the total cohort. Just over one quarter of the pedigrees in this cohort are represented by a

single sample and as such, the identification of *P2RX4* variants may have been precluded, particularly if they exhibit a very low minor allele frequency or are more commonly associated with particular pedigrees.

The unique establishment of dogs as close human companions and the high level of sequence identity between the two species has resulted in the recognition of dogs as natural models of human ageing and disease (Sandor & Kubinyi, 2019). This, in part, can be attributed to breeding programs and implementation of veterinary medicine, resulting in aged canine populations, and with this, diseases that are prevalent in aged human populations like chronic pain, inflammation, and neurodegenerative diseases. P2X4 has known roles in controlling inflammation, chronic pain, remyelination and pulse pressure in humans and rodents (Bernier, Ase *et al.*, 2018; Stokes, Scurrah *et al.*, 2011; Su, Wu *et al.*, 2019; Zabala, Vazquez-Villoldo *et al.*, 2018). The current functional characterisation of canine P2X4 suggests potential roles in canine physiology and disease. However, expression of P2X4 in canine tissues is limited to P2X4 transcripts reported in brain and gastrointestinal tissue from dogs (Lee, Ro *et al.*, 2005) and P2X4 protein detected in dog arteries (Delorey, Clifford *et al.*, 2012). Thus, future studies would benefit from utilising known P2X4 expression patterns in human and rodent tissues such as blood vessels, brain, gut, lungs and immune cells (Burnstock & Knight, 2004), to aid in identifying canine tissues that express P2X4.

P2X4 is an important signalling molecule with potential for therapeutic targeting for the treatment of major health issues including chronic pain, nerve damage and cardiovascular disease. The data presented here will aid the development of more potent and selective P2X4-targetting compounds, and will assist with pre-clinical validation of potential therapeutics for P2X4-related diseases in both human and veterinary medicine.

Declaration of transparency and scientific rigour

This Declaration acknowledges that this paper adheres to the principles for transparent reporting and scientific rigour of preclinical research as stated in the BJP guidelines for Design & Analysis, Immunoblotting and Immunochemistry, and Animal Experimentation, and as recommended by funding agencies, publishers and other organisations engaged with supporting research.

References

Abdelrahman, A., Namasivayam, V., Hinz, S., Schiedel, A. C., Kose, M., Burton, M., . . . Muller, C. E. (2017). Characterization of P2X4 receptor agonists and antagonists by calcium influx and radioligand binding studies. *Biochemical Pharmacology, 125*, 41-54. doi:10.1016/j.bcp.2016.11.016

Alexander, S. P. H., Mathie, A., Peters, J. A., Veale, E. L., Striessnig, J., Kelly, E., . . . Collaborators, C. (2019). THE CONCISE GUIDE TO PHARMACOLOGY 2019/20: Ion channels. *British Journal of Pharmacology, 176*(S1), S142-S228. doi:10.1111/bph.14749

Alexander, S. P. H., Roberts, R. E., Broughton, B. R. S., Sobey, C. G., George, C. H., Stanford, S. C., . . . Ahluwalia, A. (2018). Goals and practicalities of immunoblotting and immunohistochemistry: A guide for submission to the British Journal of Pharmacology. *British Journal of Pharmacology, 175*(3), 407-411. doi:10.1111/bph.14112

Armstrong, J. F., Faccenda, E., Harding, S. D., Pawson, A. J., Southan, C., Sharman, J. L., . . . Nc, I. (2020). The IUPHAR/BPS Guide to PHARMACOLOGY in 2020: extending immunopharmacology content and introducing the IUPHAR/MMV Guide to MALARIA PHARMACOLOGY. *Nucleic acids research, 48*(D1), D1006-D1021. doi:10.1093/nar/gkz951

Ase, A. R., Honson, N. S., Zaghdane, H., Pfeifer, T. A., & Seguela, P. (2015). Identification and Characterization of a Selective Allosteric Antagonist of Human P2X4 Receptor Channels. *Molecular Pharmacology, 87*(4), 606-616. doi:10.1124/mol.114.096222

Ase, A. R., Therrien, E., & Seguela, P. (2019). An Allosteric Inhibitory Site Conserved in the Ectodomain of P2X Receptor Channels. *Frontiers in Cellular Neuroscience, 13*, 121. doi:10.3389/fncel.2019.00121

Balazs, B., Danko, T., Kovacs, G., Koles, L., Hediger, M. A., & Zsembery, A. (2013). Investigation of the inhibitory effects of the benzodiazepine derivative, 5-BDBD on P2X4 purinergic receptors by two complementary methods. *Cellular Physiology and Biochemistry: International Journal of Experimental Cellular Physiology, Biochemistry, and Pharmacology, 32*(1), 11-24. doi:10.1159/000350119

Bernier, L. P., Ase, A. R., & Seguela, P. (2018). P2X receptor channels in chronic pain pathways. *British Journal of Pharmacology, 175*(12), 2219-2230. doi:10.1111/bph.13957

Bianchi, B. R., Lynch, K. J., Touma, E., Niforatos, W., Burgard, E. C., Alexander, K. M., . . . van Biesen, T. (1999). Pharmacological characterization of recombinant human and rat P2X receptor subtypes. *European Journal of Pharmacology, 376*(1–2), 127-138. doi:10.1016/s0014-2999(99)00350-7

Browne, L. E., Jiang, L.-H., & North, R. A. (2010). New structure enlivens interest in P2X receptors. *Trends in Pharmacological Sciences, 31*(5), 229-237. doi:10.1016/j.tips.2010.02.004

Burnstock, G., & Knight, G. E. (2004). Cellular distribution and functions of P2 receptor subtypes in different systems. *Int Rev Cytol, 240*, 31-304. doi:10.1016/s0074-7696(04)40002-3

Carpenter, D., Meadows, H. J., Brough, S., Chapman, G., Clarke, C., Coldwell, M., . . . Sanger, G. J. (1999). Site-specific splice variation of the human P2X4 receptor. *Neuroscience Letters, 273*(3), 183-186. doi:10.1016/s0304-3940(99)00653-9

Chataigneau, T., Lemoine, D., & Grutter, T. (2013). Exploring the ATP-binding site of P2X receptors. *Frontiers in Cellular Neuroscience, 7*, 273. doi:10.3389/fncel.2013.00273

Coddou, C., Sandoval, R., Hevia, M. J., & Stojilkovic, S. S. (2019). Characterization of the antagonist actions of 5-BDBD at the rat P2X4 receptor. *Neuroscience Letters, 690*, 219-224. doi:10.1016/j.neulet.2018.10.047

Curtis, M. J., Alexander, S., Cirino, G., Docherty, J. R., George, C. H., Giembycz, M. A., . . . Ahluwalia, A. (2018). Experimental design and analysis and their reporting II: updated and simplified guidance for authors and peer reviewers. *British Journal of Pharmacology, 175*(7), 987-993. doi:10.1111/bph.14153

Delorey, D. S., Clifford, P. S., Mittelstadt, S., Anton, M. M., Kluess, H. A., Tune, J. D., . . . Buckwalter, J. B. (2012). The effect of aging on adrenergic and nonadrenergic receptor expression and responsiveness in canine skeletal muscle. *Journal of applied physiology (Bethesda, Md. : 1985), 112*(5), 841-848. doi:10.1152/japplphysiol.00945.2011

Garcia-Guzman, M., Soto, F., Gomez-Hernandez, J. M., Lund, P. E., & Stuhmer, W. (1997). Characterization of recombinant human P2X4 receptor reveals pharmacological differences to the rat homologue. *Molecular Pharmacology, 51*(1), 109-118. doi:10.1124/mol.51.1.109

Gu, B. J., Baird, P. N., Vessey, K. A., Skarratt, K. K., Fletcher, E. L., Fuller, S. J., . . . Wiley, J. S. (2013). A rare functional haplotype of the P2RX4 and P2RX7 genes leads to loss of innate phagocytosis and confers increased risk of age-related macular degeneration. *Faseb Journal, 27*(4), 1479-1487. doi:10.1096/fj.12-215368

Hattori, M., & Gouaux, E. (2012). Molecular mechanism of ATP binding and ion channel activation in P2X receptors. *Nature, 485*(7397), 207-212. doi:10.1038/nature11010.

He, M.-L., Gonzalez-Iglesias, A. E., & Stojilkovic, S. S. (2003). Role of Nucleotide P2 Receptors in Calcium Signaling and Prolactin Release in Pituitary Lactotrophs. *The Journal of Biological Chemistry, 278*(47), 46270-46277. doi:10.1074/jbc.M309005200

Heusinkveld, H. J., & Westerink, R. H. (2011). Caveats and limitations of plate reader-based high-throughput kinetic measurements of intracellular calcium levels. *Toxicology and Applied Pharmacology, 255*(1), 1-8. doi:10.1016/j.taap.2011.05.020

Huang, P., Zou, Y., Zhong, X. Z., Cao, Q., Zhao, K., Zhu, M. X., . . . Dong, X. P. (2014). P2X4 forms functional ATP-activated cation channels on lysosomal membranes regulated by luminal pH. *The Journal of Biological Chemistry, 289*(25), 17658-17667. doi:10.1074/jbc.M114.552158

Huynh, N., Arabian, N., Naito, A., Louie, S., Jakowec, M. W., Asatryan, L., & Davies, D. L. (2016). Preclinical development of moxidectin as a novel therapeutic for alcohol use disorder. *Neuropharmacology, 113*(Pt A), 60-70. doi:10.1016/j.neuropharm.2016.09.016

Iyengar, S., Webster, A. A., Hemrick-Luecke, S. K., Xu, J. Y., & Simmons, R. M. (2004). Efficacy of duloxetine, a potent and balanced serotonin-norepinephrine reuptake inhibitor in persistent pain models in rats. *The Journal of Pharmacology and Experimental Therapeutics, 311*(2), 576-584. doi:10.1124/jpet.104.070656

Jelinkova, I., Yan, Z., Liang, Z., Moonat, S., Teisinger, J., Stojilkovic, S. S., & Zemkova, H. (2006). Identification of P2X4 receptor-specific residues contributing to the ivermectin effects on channel deactivation. *Biochemical and Biophysical Research Communications, 349*(2), 619-625. doi:10.1016/j.bbrc.2006.08.084

Jiang, L.-H., & Roger, S. (2020). Heterologous Expression and Patch-Clamp Recording of P2X Receptors in HEK293 Cells. *Methods in molecular biology (Clifton, N.J.), 2041*, 261-273. doi:10.1007/978-1-4939-9717-6_19

Jiang, L. H., Rassendren, F., Surprenant, A., & North, R. A. (2000). Identification of amino acid residues contributing to the ATP-binding site of a purinergic P2X receptor. *The*

Journal of Biological Chemistry, 275(44), 34190-34196. doi:10.1074/jbc.M005481200

Jones, C. A., Chessell, I. P., Simon, J., Barnard, E. A., Miller, K. J., Michel, A. D., & Humphrey, P. P. A. (2000). Functional characterization of the P2X4 receptor orthologues. *British Journal of Pharmacology, 129*(2), 388-394. doi:10.1038/sj.bjp.0703059

Kawate, T., Michel, J. C., Birdsong, W. T., & Gouaux, E. (2009). Crystal structure of the ATP-gated P2X4 ion channel in the closed state. *Nature, 460*(7255), 592-598. doi:10.1038/nature08198

Khakh, B. S., Proctor, W. R., Dunwiddie, T. V., Labarca, C., & Lester, H. A. (1999). Allosteric control of gating and kinetics at P2X(4) receptor channels. *The Journal of Neuroscience, 19*(17), 7289-7299. doi:10.1523/jneurosci.19-17-07289.1999

Layhadi, J. A., & Fountain, S. J. (2017). P2X4 Receptor-Dependent Ca2+ Influx in Model Human Monocytes and Macrophages. *International Journal of Molecular Sciences, 18*(11). doi:10.3390/ijms18112261

Layhadi, J. A., Turner, J., Crossman, D., & Fountain, S. J. (2018). ATP Evokes Ca(2+) Responses and CXCL5 Secretion via P2X4 Receptor Activation in Human Monocyte-Derived Macrophages. *J Immunol, 200*(3), 1159-1168. doi:10.4049/jimmunol.1700965

Ledderose, C., Liu, K., Kondo, Y., Slubowski, C. J., Dertnig, T., Denicoló, S., . . . Junger, W. G. (2018). Purinergic P2X4 receptors and mitochondrial ATP production regulate T cell migration. *The Journal of Clinical Investigation, 128*(8), 3583-3594. doi:10.1172/JCI120972

Lee, H. K., Ro, S., Kathy, K. D., Kim, Y. H., Kim, H. W., Horowitz, B., & Sanders, K. M. (2005). Differential expression of P2X-purinoceptor subtypes in circular and longitudinal muscle of canine colon. *Neurogastroenterology and Motility, 17*(4), 575-584. doi:10.1111/j.1365-2982.2005.00670.x

Lindblad-Toh, K., Wade, C. M., Mikkelsen, T. S., Karlsson, E. K., Jaffe, D. B., Kamal, M., . . . Lander, E. S. (2005). Genome sequence, comparative analysis and haplotype structure of the domestic dog. *Nature, 438*(7069), 803-819. doi:10.1038/nature04338

Ma, W., Hui, H., Pelegrin, P., & Surprenant, A. (2009). Pharmacological Characterization of Pannexin-1 Currents Expressed in Mammalian Cells. *Journal of Pharmacology and Experimental Therapeutics, 328*(2), 409. doi:10.1124/jpet.108.146365

Mahaut-Smith, M. P., Ennion, S. J., Rolf, M. G., & Evans, R. J. (2000). ADP is not an agonist at P2X(1) receptors: evidence for separate receptors stimulated by ATP and ADP on human platelets. *British Journal of Pharmacology, 131*(1), 108-114. doi:10.1038/sj.bjp.0703517

Micklewright, J. J., Layhadi, J. A., & Fountain, S. J. (2018). P2Y12 receptor modulation of ADP-evoked intracellular Ca(2+) signalling in THP-1 human monocytic cells. *British Journal of Pharmacology, 175*(12), 2483-2491. doi:10.1111/bph.14218

Murrell-Lagnado, R. D., & Frick, M. (2019). P2X4 and lysosome fusion. *Current Opinion in Pharmacology, 47*, 126-132. doi:10.1016/j.coph.2019.03.002

Nagata, K., Imai, T., Yamashita, T., Tsuda, M., Tozaki-Saitoh, H., & Inoue, K. (2009). Antidepressants inhibit P2X4 receptor function: a possible involvement in neuropathic pain relief. *Molecular Pain, 5*, 20. doi:10.1186/1744-8069-5-20

Ostrander, E. A., Wayne, R. K., Freedman, A. H., & Davis, B. W. (2017). Demographic history, selection and functional diversity of the canine genome. *Nature Reviews Genetics, 18*(12), 705-720. doi:10.1038/nrg.2017.67

Paredes, R. M., Etzler, J. C., Watts, L. T., & Lechleiter, J. D. (2008). Chemical Calcium Indicators. *Methods (San Diego, Calif.), 46*(3), 143-151. doi:10.1016/j.ymeth.2008.09.025

Pasqualetto, G., Brancale, A., & Young, M. T. (2018). The Molecular Determinants of Small-Molecule Ligand Binding at P2X Receptors. *Frontiers in Pharmacology, 9*, 58. doi:10.3389/fphar.2018.00058

Popova, M., Trudell, J., Li, K., Alkana, R., Davies, D., & Asatryan, L. (2013). Tryptophan 46 is a site for ethanol and ivermectin action in P2X4 receptors. *Purinergic Signal, 9*(4), 621-632. doi:10.1007/s11302-013-9373-4

Priel, A., & Silberberg, S. D. (2004). Mechanism of ivermectin facilitation of human P2X4 receptor channels. *The Journal of General Physiology, 123*(3), 281-293. doi:10.1085/jgp.200308986

Qureshi, O. S., Paramasivam, A., Yu, J. C., & Murrell-Lagnado, R. D. (2007). Regulation of P2X4 receptors by lysosomal targeting, glycan protection and exocytosis. *Journal of Cell Science, 120*(Pt 21), 3838-3849. doi:10.1242/jcs.010348

Roberts, J. A., Digby, H. R., Kara, M., El Ajouz, S., Sutcliffe, M. J., & Evans, R. J. (2008). Cysteine substitution mutagenesis and the effects of methanethiosulfonate reagents at P2X2 and P2X4 receptors support a core common mode of ATP action at P2X receptors. *The Journal of Biological Chemistry, 283*(29), 20126-20136. doi:10.1074/jbc.M800294200

Sadovnick, A. D., Gu, B. J., Traboulsee, A. L., Bernales, C. Q., Encarnacion, M., Yee, I. M., . . . Vilarino-Guell, C. (2017). Purinergic receptors P2RX4 and P2RX7 in familial multiple sclerosis. *Human Mutation, 38*(6), 736-744. doi:10.1002/humu.23218

Sandor, S., & Kubinyi, E. (2019). Genetic Pathways of Aging and Their Relevance in the Dog as a Natural Model of Human Aging. *Front Genet, 10*, 948. doi:10.3389/fgene.2019.00948

Schachter, J. B., Sromek, S. M., Nicholas, R. A., & Harden, T. K. (1997). HEK293 human embryonic kidney cells endogenously express the P2Y1 and P2Y2 receptors. *Neuropharmacology, 36*(9), 1181-1187. doi:10.1016/s0028-3908(97)00138-x

Sophocleous, R. A., Sluyter, V., Curtis, B. L., Curtis, S. J., Jurak, L. M., Faulks, M., . . . Sluyter, R. (2019). Association of a P2RX7 gene missense variant with brachycephalic dog breeds. *Animal Genetics, n/a*(n/a). doi:10.1111/age.12884

Soto, F., Garcia-Guzman, M., Gomez-Hernandez, J. M., Hollmann, M., Karschin, C., & Stuhmer, W. (1996). P2X4: an ATP-activated ionotropic receptor cloned from rat brain. *Proceedings of the National Academy of Sciences of the United States of America, 93*(8), 3684-3688. doi:10.1073/pnas.93.8.3684

Spildrejorde, M., Bartlett, R., Stokes, L., Jalilian, I., Peranec, M., Sluyter, V., . . . Sluyter, R. (2014). R270C polymorphism leads to loss of function of the canine P2X7 receptor. *Physiological Genomics, 46*(14), 512-522. doi:10.1152/physiolgenomics.00195.2013

Stokes, L., Fuller, S. J., Sluyter, R., Skarratt, K. K., Gu, B. J., & Wiley, J. S. (2010). Two haplotypes of the P2X(7) receptor containing the Ala-348 to Thr polymorphism exhibit a gain-of-function effect and enhanced interleukin-1beta secretion. *Faseb Journal, 24*(8), 2916-2927. doi:10.1096/fj.09-150862

Stokes, L., Layhadi, J. A., Bibic, L., Dhuna, K., & Fountain, S. J. (2017). P2X4 Receptor Function in the Nervous System and Current Breakthroughs in Pharmacology. *Frontiers in Pharmacology, 8*, 291. doi:10.3389/fphar.2017.00291

Stokes, L., Scurrah, K., Ellis, J. A., Cromer, B. A., Skarratt, K. K., Gu, B. J., . . . Wiley, J. S. (2011). A loss-of-function polymorphism in the human P2X4 receptor is associated with increased pulse pressure. *Hypertension, 58*(6), 1086-1092. doi:10.1161/hypertensionaha.111.176180

Stokes, L., & Surprenant, A. (2009). Dynamic regulation of the P2X4 receptor in alveolar macrophages by phagocytosis and classical activation. *European Journal of Immunology, 39*(4), 986-995. doi:10.1002/eji.200838818

Su, W. F., Wu, F., Jin, Z. H., Gu, Y., Chen, Y. T., Fei, Y., . . . Chen, G. (2019). Overexpression of P2X4 receptor in Schwann cells promotes motor and sensory functional recovery and remyelination via BDNF secretion after nerve injury. *Glia, 67*(1), 78-90. doi:10.1002/glia.23527

Tian, M., Abdelrahman, A., Weinhausen, S., Hinz, S., Weyer, S., Dosa, S., . . . Muller, C. E. (2014). Carbamazepine derivatives with P2X4 receptor-blocking activity. *Bioorganic and Medicinal Chemistry, 22*(3), 1077-1088. doi:10.1016/j.bmc.2013.12.035

Trang, T., Beggs, S., Wan, X., & Salter, M. W. (2009). P2X4-receptor-mediated synthesis and release of brain-derived neurotrophic factor in microglia is dependent on calcium and p38-mitogen-activated protein kinase activation. *The Journal of Neuroscience, 29*. doi:10.1523/JNEUROSCI.5714-08.2009

Trang, T., & Salter, M. W. (2012). P2X4 purinoceptor signaling in chronic pain. *Purinergic Signalling, 8*(3), 621-628. doi:10.1007/s11302-012-9306-7

Tsuda, M., Tozaki-Saitoh, H., & Inoue, K. (2010). Pain and purinergic signaling. *Brain Research Reviews, 63*(1-2), 222-232. doi:10.1016/j.brainresrev.2009.11.003

Tvrdonova, V., Rokic, M. B., Stojilkovic, S. S., & Zemkova, H. (2014). Identification of Functionally Important Residues of the Rat P2X4 Receptor by Alanine Scanning Mutagenesis of the Dorsal Fin and Left Flipper Domains. *PLoS One, 9*(11), e112902. doi:10.1371/journal.pone.0112902

Ulmann, L., Hatcher, J. P., Hughes, J. P., Chaumont, S., Green, P. J., Conquet, F., . . . Rassendren, F. (2008). Up-Regulation of P2X(4) Receptors in Spinal Microglia after Peripheral Nerve Injury Mediates BDNF Release and Neuropathic Pain. *The Journal of Neuroscience, 28*(44), 11263-11268. doi:10.1523/jneurosci.2308-08.2008

Ulmann, L., Hirbec, H., & Rassendren, F. (2010). P2X4 receptors mediate PGE2 release by tissue-resident macrophages and initiate inflammatory pain. *The EMBO Journal, 29*(14), 2290-2300. doi:10.1038/emboj.2010.126

Vandevelde, M., & Zurbriggen, A. (2005). Demyelination in canine distemper virus infection: a review. *Acta Neuropathol, 109*(1), 56-68. doi:10.1007/s00401-004-0958-4

Yamamoto, K., Korenaga, R., Kamiya, A., Qi, Z., Sokabe, M., & Ando, J. (2000). P2X(4) receptors mediate ATP-induced calcium influx in human vascular endothelial cells. *American Journal of Physiology. Heart and Circulatory Physiology, 279*(1), H285-292. doi:10.1152/ajpheart.2000.279.1.H285

Yamamoto, K., Sokabe, T., Matsumoto, T., Yoshimura, K., Shibata, M., Ohura, N., . . . Ando, J. (2006). Impaired flow-dependent control of vascular tone and remodeling in P2X4-deficient mice. *Nature Medicine, 12*(1), 133-137. doi:10.1038/nm1338

Yamashita, T., Yamamoto, S., Zhang, J., Kometani, M., Tomiyama, D., Kohno, K., . . . Tsuda, M. (2016). Duloxetine Inhibits Microglial P2X4 Receptor Function and Alleviates Neuropathic Pain after Peripheral Nerve Injury. *PLoS One, 11*(10), e0165189. doi:10.1371/journal.pone.0165189

Zabala, A., Vazquez-Villoldo, N., Rissiek, B., Gejo, J., Martin, A., Palomino, A., . . . Domercq, M. (2018). P2X4 receptor controls microglia activation and favors remyelination in autoimmune encephalitis. *EMBO Molecular Medicine, 10*(8), e8743. doi:10.15252/emmm.201708743

Zarei, M., Sabetkasaei, M., & Moini Zanjani, T. (2014). Paroxetine Attenuates the Development and Existing Pain in a Rat Model of Neurophatic Pain. *Iranian Biomedical Journal, 18*(2), 94-100. doi:10.6091/ibj.1282.2013

Table 1. Distribution of canine *P2RX4* exon variants in our cohort of dog samples.

Variant	Allele change	cDNA position	n	Genotype		Allele frequency	Prevalence
				Wild-type (n)	Mutant[a] (n)		
Observed variants[b]							
C5C	tgC>tgT	15	63	55	8	0.063	12.7%
T266T	acC>acT	798	88	85	3	0.017	3.4%
Reported variants[c]							
A9D	gcC>gcA	26	63	55	0	ND	ND
R231C	Cgt>Tgt	691	90	90	0	ND	ND
L345V	Ctc>Gtc	1033	82	82	0	ND	ND

[a]Only heterozygous variants were observed in this cohort

[b]Variants that were observed at least once in our cohort

[c]Variants reported previously in either dbSNP, EVA or iDOG databases but not observed in this study

ND, not detected

Table 2. Sequence identity between protein sequences of cloned P2X4 orthologues.

	Sequence identity (%)						
	Canine[a]	Human[b]	Bovine[c]	Mouse[d]	Rat[e]	*Xenopus*[f]	Zebrafish[g]
Canine	100	90	88.7	86.1	85.6	69.5	56.5
Human		100	87.4	86.9	87.4	69.7	58.3
Bovine			100	85.6	85.8	68.2	56.5
Mouse				100	95.6	67.7	57.8
Rat					100	68.2	59.1
Xenopus						100	56.6
Zebrafish							100

Sequences were obtained from the NCBI protein database with the exception of the full length canine P2X4 sequence which was unavailable from NCBI and was retrieved from ENSEMBL. Sequences were aligned with Clustal O (v1.2.4) and sequence identity determined using the percent identity matrix tool. [a]ENSCAFT00000013312.3, [b]NP_002551.2, [c]NP_001029221.1, [d]NP_035156.2, [e]NP_113782.1, [f]NP_001082067.1, [g]NP_705939.1.

Table 3. Pharmacological activity of compounds mediating changes in intracellular Ca^{2+} in 1321N1 cells expressing canine or human P2X4.

	Canine P2X4		Human P2X4	
	pEC_{50} or pIC_{50}	Hill coefficient	pEC_{50} or pIC_{50}	Hill coefficient
Agonists (pEC_{50})[a]				
ATP	6.59 ± 0.13	1.89	6.72 ± 0.06	1.59
BzATP	3.44 ± 0.13*† (41%)	1.72	5.04 ± 0.26† (92%)	1.68
ADP[b]	N.R (<10%)	-	N.R. (<10%)	-
Modulators (pEC_{50})[c]				
IVM	6.98 ± 0.05† (111%)	1.60	6.91 ± 0.13† (137%)	1.85
ATP	6.52 ± 0.12	2.09	6.69 ± 0.07	1.66
Antagonists (pIC_{50})[d]				
BX 430	5.11 ± 0.06* (43%)	1.65	5.71 ± 0.08 (29%)	1.29
5-BDBD	5.24 ± 0.24 (53%)	0.89	5.28 ± 0.36 (54%)	0.99
Duloxetine	4.82 ± 0.20 (13%)	1.00	4.77 ± 0.18 (13%)	1.00
Paroxetine	4.88 ± 0.13* (28%)	0.76	4.11 ± 0.20 (37%)	0.84
TNP-ATP	5.09 ± 0.27 (18%)	1.00	5.36 ± 0.24 (8%)	1.00

[a]Values in parentheses indicate the percent of max response compared to 10 μM ATP. [b]ADP in the presence of hexokinase to remove contaminating ATP. [c]pEC_{50} of ATP in the absence or presence of 3 μM IVM; values in parentheses indicate the percent of response compared to 10 μM ATP. [d]pIC_{50} of antagonists calculated using the approximate pEC_{80} of ATP (0.75 μM); values in parentheses indicate the percent of response in the presence of 100 μM antagonist compared to max ATP in absence of antagonist. N.R. negligible response (pEC_{50} not calculated). *$P < 0.05$ compared to the pEC_{50} or pIC_{50} of respective compound at human P2X4; †$P < 0.05$ compared to ATP alone for corresponding P2X4 (non-parametric Mann-Whitney U test for agonists and IVM, parametric Student's t-test for antagonists). Data are mean ± SEM from five independent experiments.

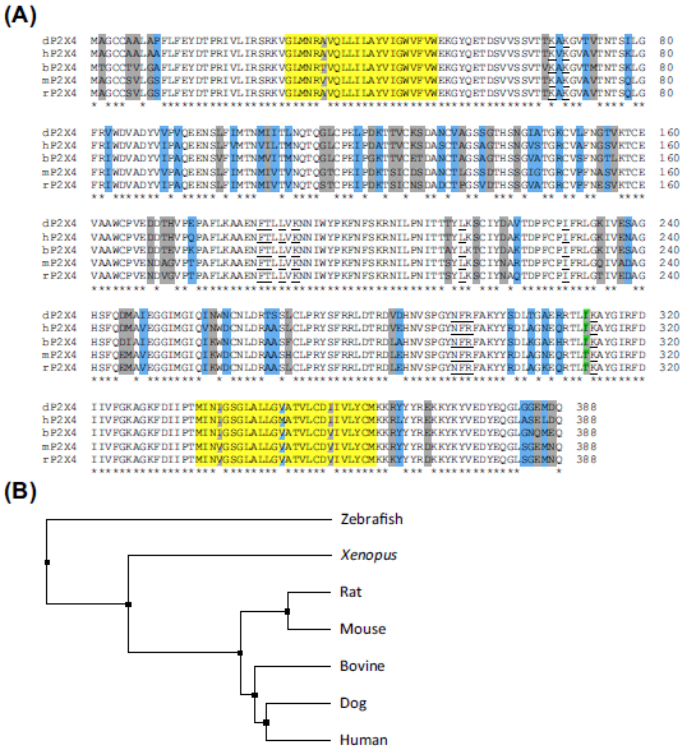

Figure 1. Multiple sequence alignment of known mammalian P2X4 receptors. (A) P2X4 sequences were aligned using Clustal O v1.2.4 (https://www.ebi.ac.uk/Tools/msa/clustalo/; last accessed November 2019). Asterisks (*) underneath the alignment indicate residues that are identical between all five orthologues and blank spaces indicate where differences are observed. Sections highlighted grey indicate where canine and human residues are identical but differ compared to other non-human orthologues, and sections highlighted blue indicate where canine and human residues differ. Predicted transmembrane domains based on the Expasy TMpred prediction program (https://www.expasy.org/; last accessed November 2019) are highlighted yellow. The amino acid residue involved in P2X4 orthologue sensitivity to the P2X4 antagonist BX430 (identified by Ase, Therrien *et al.* (2019)) is highlighted green. Residues where two of the above occur are indicated by dual-highlighted split boxes. Amino acids involved in ATP binding are underlined. Dog (dP2X4; P2RX4-201 ENSCAFT00000013312.3), human (hP2X4; NP_002551.2), bovine (bP2X4; NP_001029221.1), mouse (mP2X4; NP_035156.2) and rat (rP2X4; NP_113782.1) P2X4 protein sequence entries were obtained from ENSEMBL or NCBI (last accessed November 2019). (B) Phylogenetic tree calculated from Clustal O multiple sequence alignment of above P2X4 sequences, as well as zebrafish P2X4 (NP_705939.1) and *Xenopus* P2X4 (NP_001082067.1). Tree was constructed using the average distance method in Jalview 2.11.0.

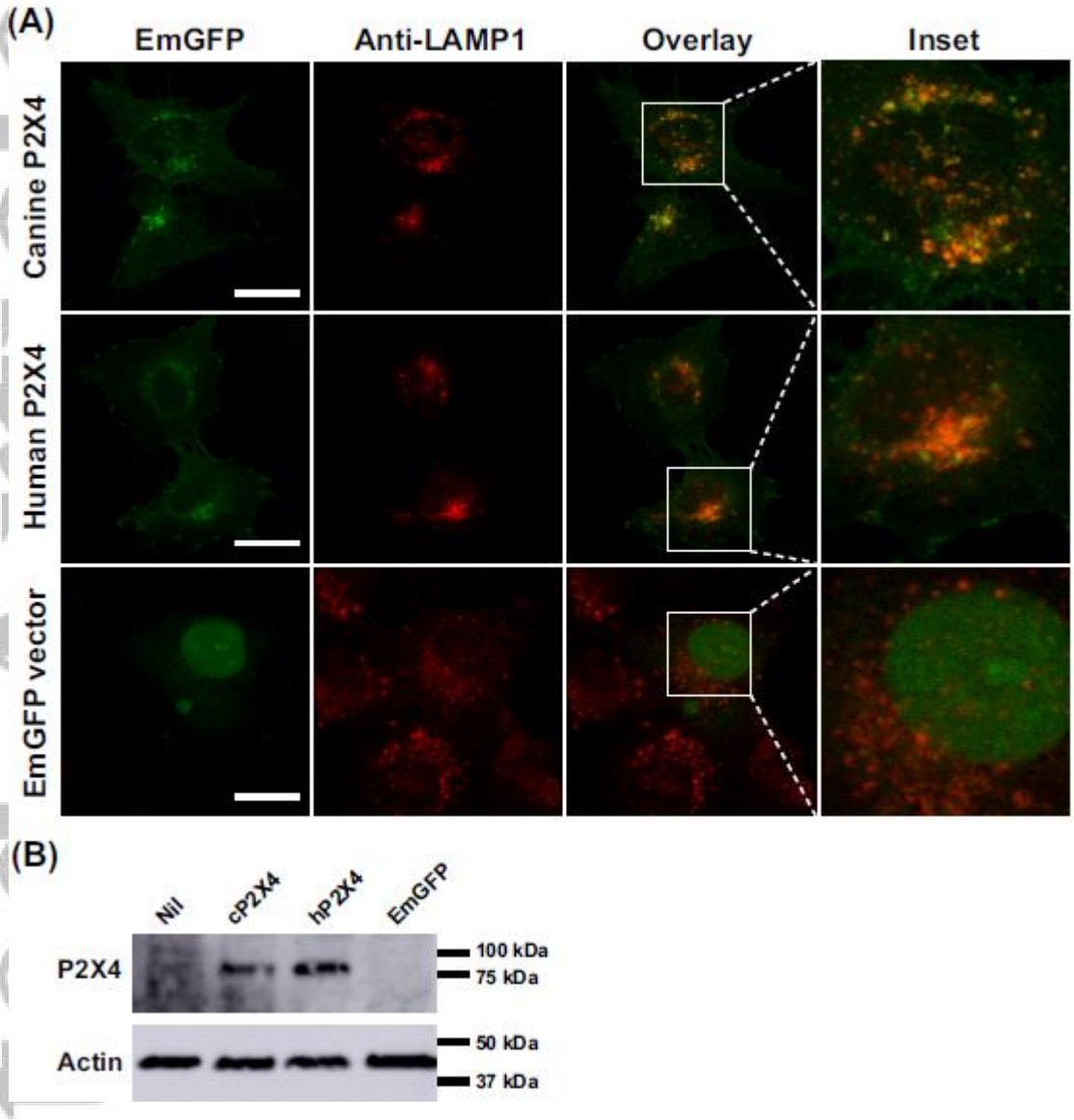

Figure 2. Expression of canine and human P2X4 in 1321N1 cells. (A) 1321N1 cells, transfected with canine or human P2X4-EmGFP, or EmGFP vector alone, were fixed, permeabilised and stained with anti-LAMP1 antibody to label lysosomes. Cells were imaged by confocal microscopy and co-localisation analysed using ImageJ. Inset squares were digitally enlarged three times the original to examine P2X4 localisation in vesicular compartments. Scale bar = 20 µm. (B) Proteins of whole cell lysates of non-transfected 1321N1 cells (Nil) and 1321N1 transfected with canine (cP2X4) or human (hP2X4) P2X4-EmGFP or EmGFP vector alone (EmGFP) were examined by western blotting using an anti-P2X4 or anti-actin antibody prior to imaging. Data are representative of three independent experiments.

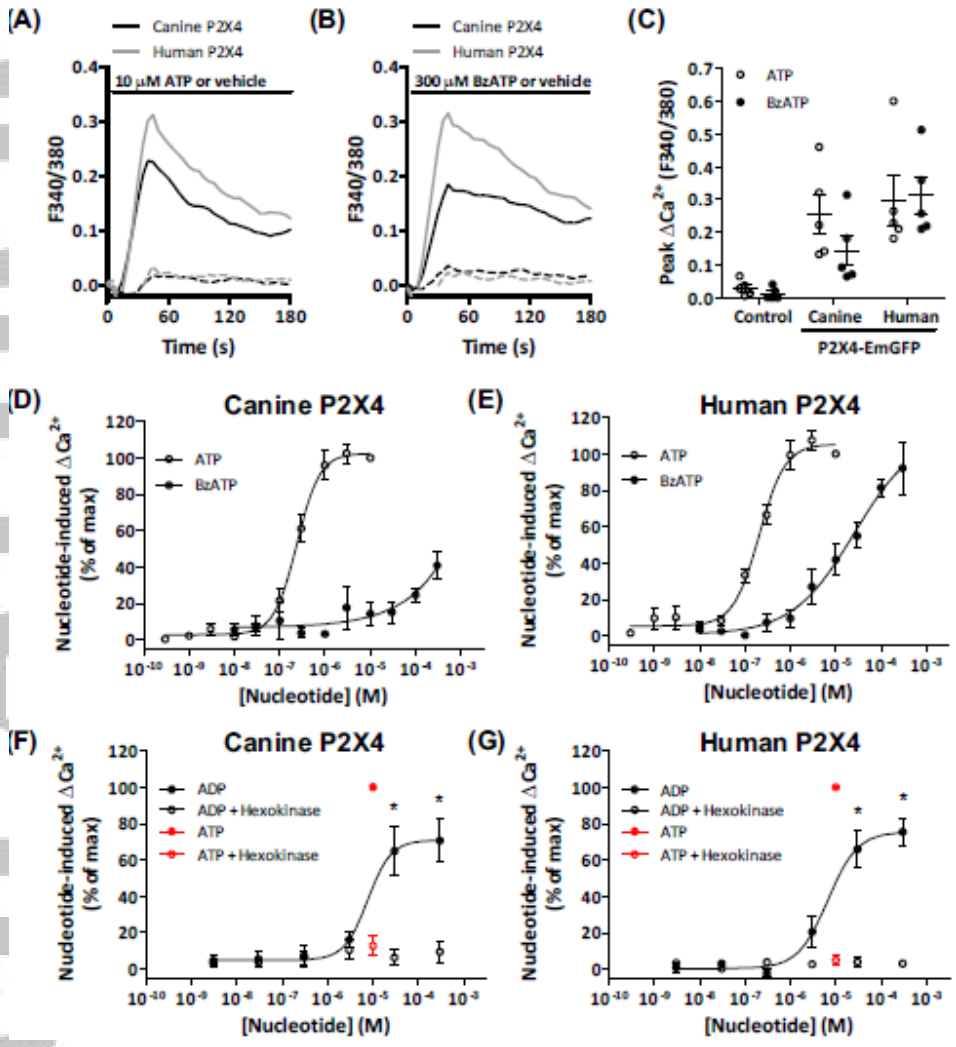

Figure 3. Ca^{2+} response agonist profile of canine and human P2X4 in 1321N1 cells. (A-G) 1321N1 cells, transfected with canine or human P2X4-EmGFP or EmGFP (control) plasmid DNA, were loaded with Fura-2 and incubated in the absence or presence of each nucleotide in ECS (as indicated). (A, B) Representative ΔCa^{2+} traces for each nucleotide at respective maximal concentration. Solid and dashed lines indicate Ca^{2+} traces in presence or absence of nucleotide, respectively. (C) Peak ΔCa^{2+} response to maximal concentrations of ATP (10 μM) and BzATP (300 μM). (D-G) Nucleotide-induced ΔCa^{2+} responses are presented as percent of maximum response to 10 μM ATP, with data fit to the Hill equation to produce concentration-response curves. (F, G) ADP or ATP were pre-incubated with hexokinase (4.5 $U.mL^{-1}$) for 1 hour at 37°C prior to addition. Red open and closed circles represent 10 μM ATP in the presence or absence of hexokinase, respectively. (A-H) Data shown are mean ± SEM from five independent experiments (or eight for ATP concentration-response curve). ***P* < 0.05 compared to nucleotide in absence of hexokinase using a two-way ANOVA with Bonferroni *post hoc* test following a D'agostino-Pearson test for normality.

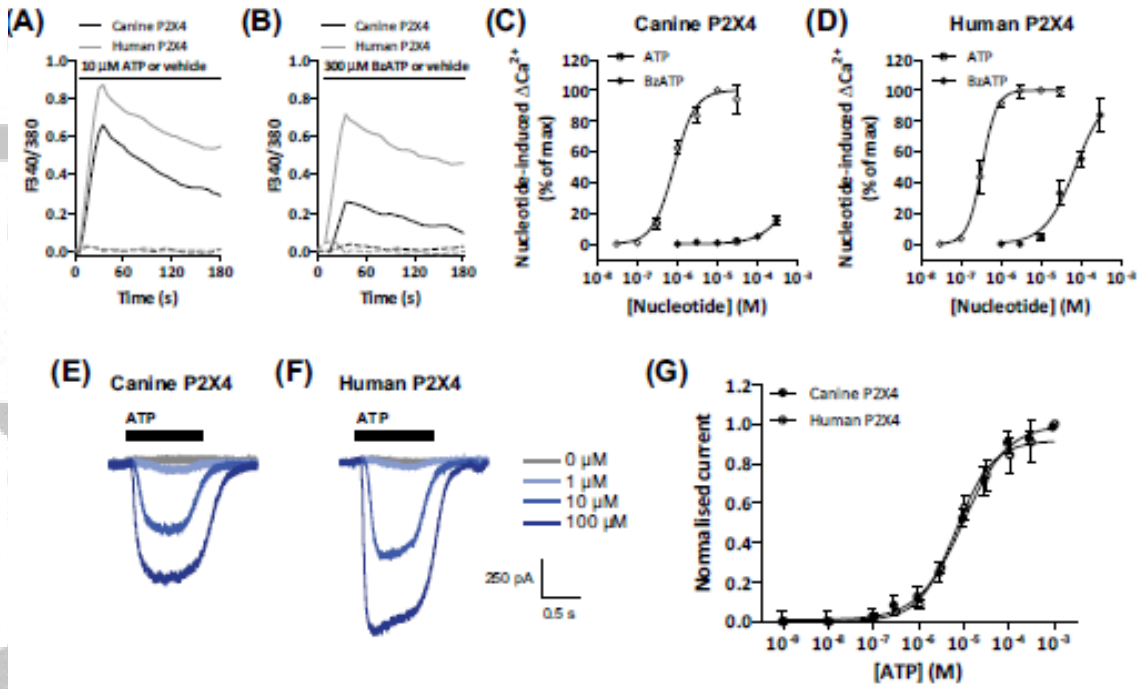

Figure 4. Agonist profile of canine and human P2X4 in HEK293 cells. (A-G) HEK293 cells, transfected with canine or human P2X4-EmGFP plasmid DNA. (A-D) Cells were loaded with Fura-2 and incubated in the absence or presence of each nucleotide (as indicated). (A, B) Representative ΔCa^{2+} traces for each nucleotide at respective maximal concentration. Solid and dashed lines indicate Ca^{2+} traces in presence or absence of nucleotide in ECS, respectively. (C, D) Nucleotide-induced ΔCa^{2+} responses are presented as percent of maximum response to 10 µM ATP. Data shown are mean ± SEM from five independent experiments. (E, F) Representative automated whole-cell patch clamp current traces of canine or human P2X4 in absence or presence of increasing concentrations of ATP (as indicated by the bars above the current traces) in standard external solution. (G) ATP-induced inward currents are presented as charge density (pC/pF) normalised to current at 1 mM ATP, with data fit to the Hill equation to produce concentration-response curves. Data shown are mean ± SEM from eight (canine P2X4) or six (human P2X4) independent experiments.

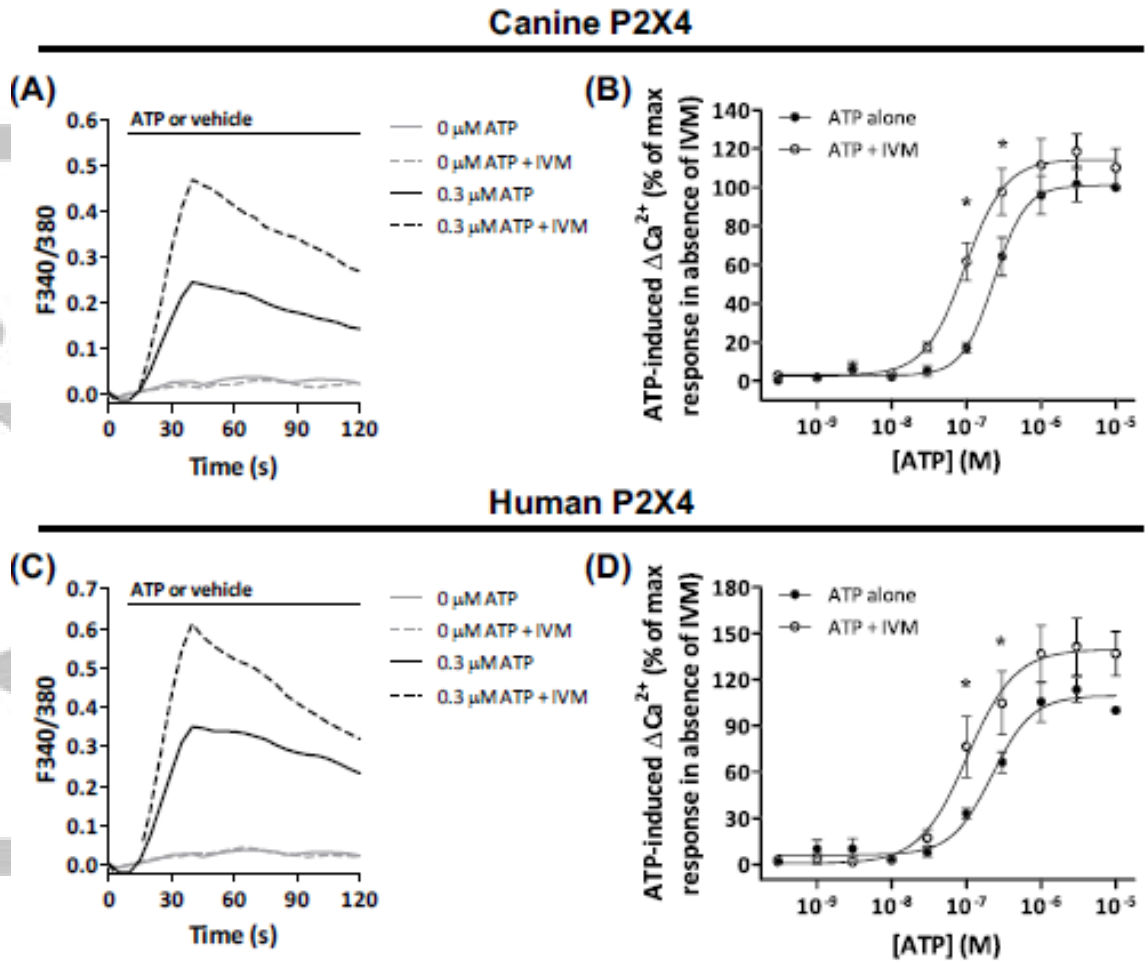

Figure 5. Modulation of ATP-induced Ca^{2+} responses by ivermectin (IVM) on canine and human P2X4 in 1321N1 cells. (A-D) 1321N1 cells, transfected with canine or human P2X4-EmGFP, were loaded with Fura-2 and pre-incubated in the absence (vehicle, 0.1% DMSO in ECS) or presence of 3 μM IVM for 20 minutes. Cells were incubated in the absence or presence of increasing concentrations of ATP. (A, C) Representative ΔCa^{2+} traces for 0.3 μM ATP, where solid and dashed lines indicate Ca^{2+} traces in absence or presence of IVM, respectively. (B, D) ATP-induced ΔCa^{2+} responses are presented as percent of maximum response to 10 μM ATP in the absence of IVM, with data fit to the Hill equation to produce concentration-response curves. (A-D) Data shown are mean ± SEM from five independent experiments. ***P* < 0.05 compared to respective ATP concentration in absence of IVM using a two-way ANOVA with Bonferroni *post hoc* test following a D'agostino-Pearson test for normality.

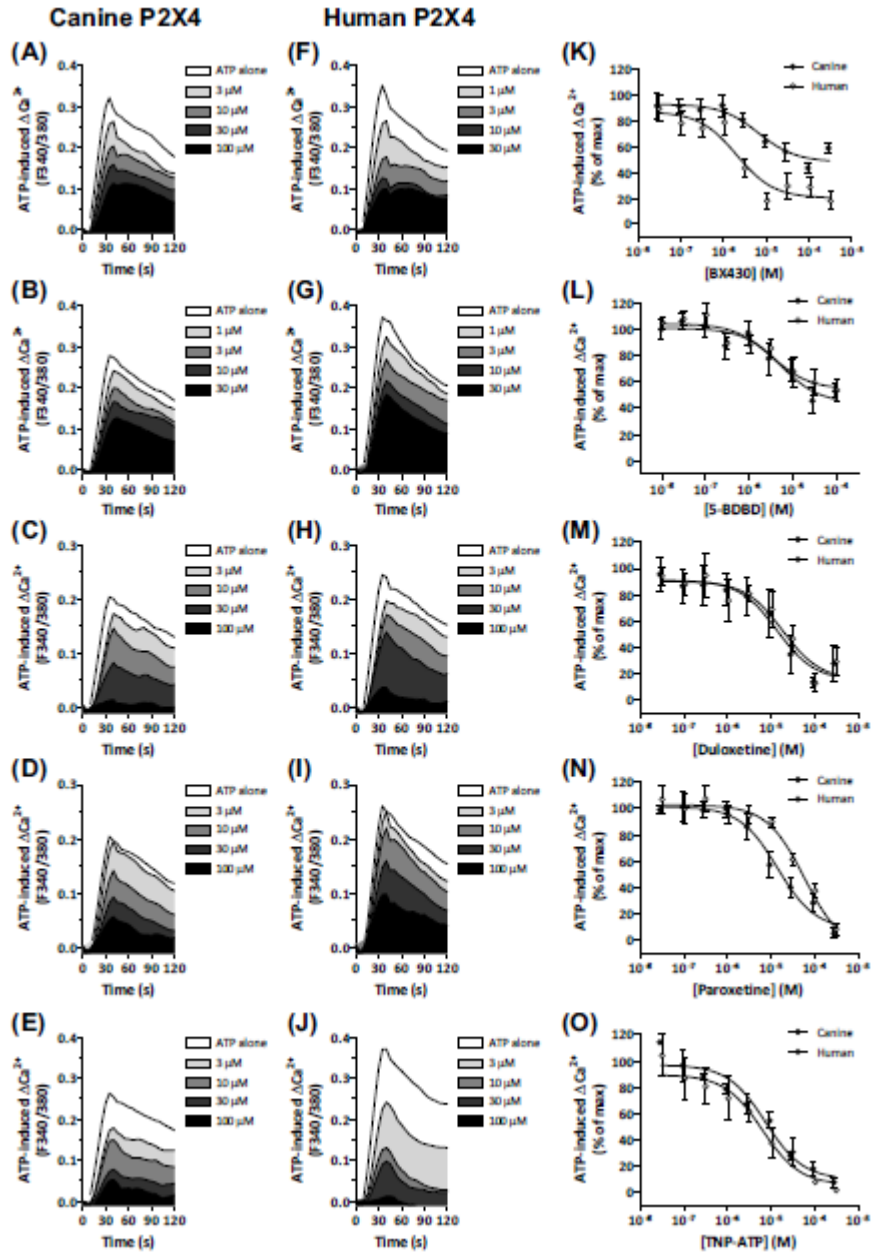

Figure 6. Ca^{2+} response antagonist profiles of canine and human P2X4 in 1321N1 cells. (A-O) 1321N1 cells, transfected with canine or human P2X4-EmGFP, were loaded with Fura-2 and incubated in the absence (ECS alone or 1% DMSO in ECS) or presence of increasing concentrations of BX430 (1% DMSO), 5-BDBD (1% DMSO), duloxetine (ECS), paroxetine (1% DMSO) or TNP-ATP (ECS) for 20 minutes and then exposed to 0.75 µM ATP (approximate to the EC_{80} of ATP). Representative ΔCa^{2+} traces in absence or presence of antagonists at (A-E) canine and (F-J) human P2X4. (K-O) ATP-induced ΔCa^{2+} responses are presented as percent of maximum response to 10 µM ATP in the absence of antagonists, with data fit to the Hill equation to produce concentration-response curves. Data points indicate the mean ± SEM from five independent experiments.

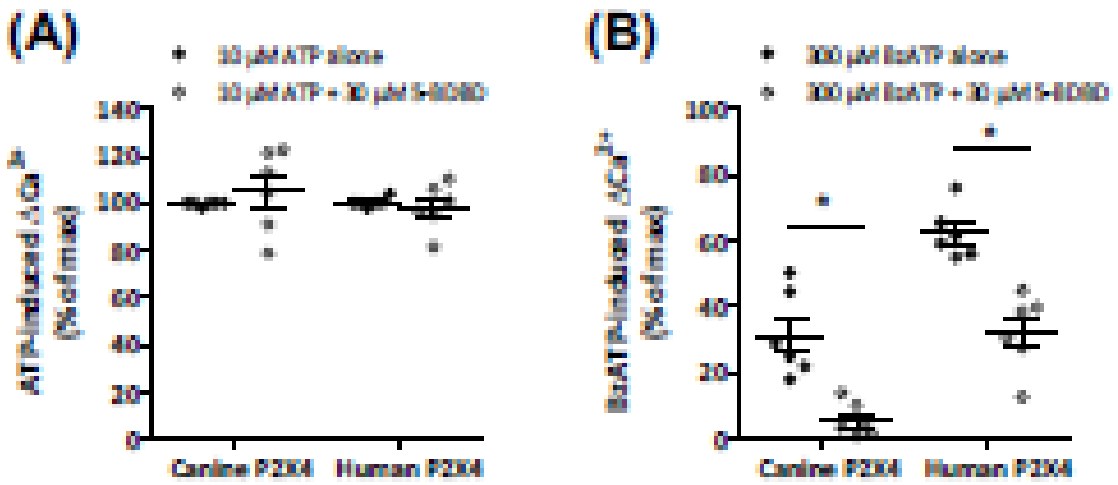

Figure 7. Inhibitory effect of 5-BDBD at maximal P2X4 agonist concentrations. (A, B) 1321N1 cells, transfected with canine or human P2X4-EmGFP, were loaded with Fura-2, pre-incubated in the absence (0.3% DMSO in ECS) or presence of 30 μM 5-BDBD for 20 minutes and then incubated with maximal or near maximal concentrations of (A) ATP or (B) BzATP, respectively. Data were plotted as a percentage of the maximal response to 10 μM ATP in absence of antagonist. Data are presented as the mean ± SEM from six independent experiments. **P* < 0.05 compared to nucleotide alone using a parametric Student's t-test.